Elsevier Editorial System(tm) for International Journal of Multiphase Flow
Manuscript Draft

Corresponding Author: Dr. Santiago Marquez Damian,

Corresponding Author's Institution: CIMEC

First Author: Santiago Marquez Damian

Order of Authors: Santiago Marquez Damian; Norberto M Nigro

Abstract: The study of multi-phase models is a field of great interest in industry and academia. Multi-phase flows are present in hydraulics, petrochemical industry, oceanography, siderurgy, atomic energy and many other human activities. This field is far from being completely understood and the available tools are still in a developing stage. Nowadays the only general model for this kind of problems are either Direct Numerical Simulation or models based in the physics of fluids. In this scenario, the aim of this work is to present a new model based on the Volume of Fluid method and the Mixture Model in order to solve multi-phase flows with different interface scales and the transition among them. The interface scale is characterized by a measure of the grid, which acts as a geometrical filter and is related with the accuracy in the solution, in this sense the presented coupled model allows to reduce the grid requirements for a given accuracy. With this objective in mind, a generalization of the Algebraic Slip Mixture Model is proposed to solve problems involving short and long scale interfaces in an unified framework. This model is implemented using the OpenFOAM(R) libraries to generate a state-of-the-art solver capable of solving large problems on High Performance Computing facilities. The proposed examples serve as a validation for the presented model and sum up in the community discussion about coupled models.

*Cover Letter

Santa Fe, Argentina, March 28ᵗʰ 2013

International Journal of Multiphase Flow

Dear Editor:

Please find attached for your kind review our manuscript entitled "An Extended Mixture Model for the Simultaneous Treatment of Short and Long Scale Interfaces".

In this work we present a coupled model for the solution of multi-phase problems with different length scales for the interfaces. The coupled model relies on the well established Volume of Fluid and Mixture models writing them in a common framework. The details for proper coupling are discussed and compared with similar methods. Here it is important to note that this topic has started to being discussed in the last years and even within this venue.

The implementation of such a coupled model is achieved by the OpenFOAM(R) libraries allowing to manage large problems in High Performance Computing facilities. The solution algorithm relies on the PISO method applied to collocated meshes and is described in great detail.

Finally, three examples are presented and solved, two of them are proposed by the authors and the left is taken from the literature in order compare with other authors in the topic. In addition, new measures are given in order to know the grade of improvement reached by the proposed method respect to other models.

Looking forward to your favorable consideration.

Most sincerely,

Santiago Márquez Damián (corresponding author, santiagomarquezd@gmail.com)
Norberto M. Nigro
Centro de Investigaciones en Mecanica Computacional (CIMEC), UNL/CONICET,

International Journal of Multiphase Flow - Highlights

"An Extended Mixture Model for the Simultaneous Treatment of Short and Long Scale Interfaces ".

> The mesh is a filter for surface capturing capabilities in VOF > We present a VOF/ASMM coupled model for mixed free surface scales > A solver is derived and implemented in OpenFOAM > Several examples are solved proposing new ones > New measures are proposed for improvement quantification

An Extended Mixture Model for the Simultaneous Treatment of Short and Long Scale Interfaces

Santiago Márquez Damián[a], Norberto M. Nigro[a]

[a]*Centro de Investigaciones en Mecánica Computacional (CIMEC), UNL/CONICET,
Colectora Ruta Nac. 168 / Paraje El Pozo, (3000) Santa Fe, Argentina,
http: // www. cimec. org. ar*

Abstract

The study of multi-phase models is a field of great interest in industry and academia. Multi-phase flows are present in hydraulics, petrochemical industry, oceanography, siderurgy, atomic energy and many other human activities. This field is far from being completely understood and the available tools are still in a developing stage. Nowadays the only general model for this kind of problems are either Direct Numerical Simulation or models based in the physics of fluids. In this scenario, the aim of this work is to present a new model based on the Volume of Fluid method and the Mixture Model in order to solve multi-phase flows with different interface scales and the transition among them. The interface scale is characterized by a measure of the grid, which acts as a geometrical filter and is related with the accuracy in the solution, in this sense the presented coupled model allows to reduce the grid requirements for a given accuracy. With this objective in mind, a generalization of the Algebraic Slip Mixture Model is proposed to solve problems involving short and long scale interfaces in an unified framework. This model is implemented using the OpenFOAM® libraries to generate a state-of-the-art solver capable of solving large problems on High Performance

Computing facilities. The proposed examples serve as a validation for the presented model and sum up in the community discussion about coupled models.

1. Introduction

The multi-fluid and multi-phase systems are often present in academia and industry, setting generally a big challenge in their solution. The correct representation and solution of this kind of systems is a key knowledge in the car, atomic energy, petrochemical, naval and hydraulics, chemistry, and other industries (Brennen, 2005; Prosperetti and Tryggvason, 2007; Kolev, 2010). Throughout the years several models have been devised to simulate these phenomena, within the most often used may be: the Direct Numerical Simulation (DNS) (Scardovelli and Zaleski, 1999), the Volume of Fluid Method (VOF) (Hirt and Nichols, 1981), the Multi-fluid Method (Drew, 1983; Ishii and Hibiki, 2010) and the Mixture Model (Manninen et al., 1996). In DNS applied to multi-phase flow the model is able to represent all the geometrical and turbulent scales for each phase. To do so, the complete set of momentum and mass conservation equation is solved for each phase, setting the corresponding interfacial and boundary conditions. It is clear that this technique is only applicable to simple real cases or laboratory tests due to the great computational resources that are required nowadays. This approach is then more suitable for cases that belong to the physics of fluids.

In the VOF Method the geometrical analysis is similar to DNS, being the

2

mesh size the parameter which determines the representation of the different scales of the problem. The turbulence is generally solved using either time filtering or spatial filtering. The time filtering is implemented by the Reynolds Averaged Navier Stokes Methods (RANS), meanwhile the spatial filtering is performed using Large Eddy Simulation (LES).

The Multi-fluid model represents the next level of simplification. In this model the contact surface between phases is not explicitly tracked, considering all phases as interpenetrating continua. This approach is generally used when the geometrical structures of the flux cannot be captured by the available mesh and/or this is not an important part of the solution process. With this aim, the mass and momentum conservation equations are solved for each solid, liquid and gas phase. The representation of phases interaction is included by means of interchange terms in the mass and momentum conservation equations.

Finally, the Mixture Model has an additional simplification, it is that all the interpenetrating phases can be considered as a mixture, solving only one momentum equation, a mass conservation equation for the mixture and a mass phase fraction equation for all but one phase. The physical properties used in the mixture equations are given by a combination of the properties of each phase, using the densities and/or volume fractions in the averaging process. In the case of this work a particular Mixture Model is used which known as the Algebraic Slip Mixture Model (ASMM) since the relative velocity needed is calculated algebraically. It is worthy to note that, even though the Mixture Model represents a simplification respect to the Multi-fluid model, the applicability of each model and the results' quality

3

strongly relies on the nature of the problem, giving similar results in many problems. In addition the Multi-fluid model has a great weakness due to its ill-posedness (Zanotti et al., 2007) and the lack of closure laws for the momentum transfer terms between phases (Manninen et al., 1996).

The VOF model is used in problems where surface capturing is crucial, with an important incidence of the surface tension and adhesion phenomena as in drop formation, capillarity and jet break-up, or where the free surface position prediction is essential, such as nozzles, free-surface problems in hydraulics, naval industry, reservoirs and liquids separation. In all of these cases the interfaces considered have long scale, taking as a reference some measure of the mesh size.

In the case of Multi-fluid and Mixture models the interest is found in the capacity of predicting the behavior of flows with small-scale interfaces –dispersed interfaces –when is not possible or desirable a complete modeling. This kind of interfaces is often found in sedimentation tanks, cyclone separators, annular flow in refineries and fine bubbles flow in heat exchangers.

As was presented, the DNS represents the only model which is capable to afford general multi-phase/fluid problems (Scardovelli and Zaleski, 1999; Tryggvason et al., 2006); nevertheless, the present computational resources limitations turn impossible its direct application. On the other hand, due to their lack of generality, the rest of the models work only in particular cases, according to each model's hypothesis.

This situation leaves an open discussion respect to the development of new models capable to manage several interface scales and/or transitions between them. So that, a new group of cases could be included such as the

annular mist flow or *droplet annular flow*, the transition from *churn flow* to *bubbly flow* (Ishii and Hibiki, 2010) citing cases from the nuclear and chemical industry or the interaction of bubble plume with a free surface as is frequent in oceanography (Friedl and Fanneløp, 2000; Cloete et al., 2009) or siderurgy (Zanotti et al., 2007; Zanotti, 2007).

The state of the art in this topic shows that the study of the so called coupled models for the treatment of short and long scale interfaces has been in discussion in the last years. The main motivation has been the lack of precision in the solutions using the known models and the solutions given by DNS limited to low Reynolds number flows. The first work in the topic seems to be that was presented by Černe *et al.* (Černe et al., 2001), where the authors introduced a coupled method between VOF and Multi-fluid (Two-fluids) model. A model switching parameter is given by a dispersion function, γ, related to the free-surface reconstruction method, so that, there is a threshold value over which the interface is treated as having long scale and captured by VOF and the opposite case with the Two-fluids model. Then, some test cases are solved comparing the convergence of a pure VOF solution against the coupled solver. Since each base model is written in its original formulation there is not an unified solution framework and it is necessary to switch between models with different number of equations. This issue has particular importance in the treatment of the velocities, since the VOF model has only one velocity field meanwhile the Two-Fluids model has one velocity field per phase. The transition from two velocities to one is managed by the definition of the velocity of center-of-volume, in the opposite case the same velocity is assigned to each phase. This assumption implies some momentum

5

equilibrium physically unrealistic and leads to lose the interface friction.

The solution of multiple scale interface problems with an unified framework was presented by Masuda and Nagaoka (Masuda and Nagaoka, 2006), who devised a coupled VOF/Multi-fluid method for the application in nozzle flows. This method recognizes four fluids, the original two fluids and two mixtures, one given by the first fluid as the dispersed phase and the other one using the second fluid as the dispersed phase. The transition between the models is governed by the dispersion function proposed by Černe *et al.*. In the same line, Štrubelj and Tiselj (Štrubelj and Tiselj, 2011), gave an unified framework for the Level-Set and the Multi-fluid method. In this approach all the scales are solved by the Multi-fluid method and an additional interface tracking term is implemented within it. The detection of the scale interfaces is achieved by the cited dispersion function.

Another example of a model based on the unified VOF/Multi-fluid approach is that was given by Yan and Che (Yan and Che, 2010). It relies on a division of the phases by their physical state and the interface lenght scale, giving three new phases: the liquid (phase 1), the large-lenght-scale-interface (LSI) with gas phase (phase 2) and the small-lenghtscale-interface (SSI) with gas phase (phase 3). So that, a shared momentum equation is solved for the mixture of phase 1 and phase 2 and a second momentum equation is solved for phase 3. This second momentum equation gives the dynamics of the particulated phase. The geometry of the interfaces is captured by a VOF method for phase 1 and 2. Phase 3 is also governed by a mass conservation equation but without interface capturing since it is considered a dispersed phase.

The concept of phase division by their physical state and lenght scale was also developed by Bohorquez (Bohorquez R. de M., 2008) for the treatment of air-water-sediments in hydraulics problems. Here, there are two principal phases, the air (phase 1) and the water-sediments mixture (phase 2), the third phase are the sediments which are dispersed within the water. Thus, a VOF/ASMM model is derived in an unified framework where the LSI between phase 1 and phase 2 is solved by the VOF model. The geometry of the dispersed phase (phase 3) is solved by an additional mass conservation equation without interface capturing. Since the whole model is given in the ASMM framework, only one momentum equation is solved for the air-water-sediments mixture.

From the study of the presented references is also noticeable that the field of coupled models for different interface length scales is still in development. The advances on the description of this kind of problems require the development and improvement of the models and the possibility of validation. The validation plays a crucial role, requiring more experiments and getting analytical or semi-analytical solutions. In this context the objective of this work is to present a VOF/ASMM coupled model for two phase problems and its application for academic and industrial problems. The derivation of the model is motivated from the analysis of VOF solutions looking for a better treatment of the unresolved interface scales.

2. Motivation

The numerical motivation for the use of coupled models rises from the careful observation of the solutions obtained with the basic models. For the

7

present work, where a VOF/ASMM coupling is proposed, the analysis starts by the VOF method which is able to capture of all the scales of the interface with the appropriate mesh. Following the concept of different length-scale in the interfaces the mesh works as a "filter" for the interface and the long and short scales can be determined. So that some results often obtained by the VOF method could be re-examined to detect such interface scales and the behavior of this method. Thus, the result of the Rayleigh-Taylor problem for $t = 5.4$ is presented in Figure 1.a), in addition the result for a mesh four times coarser is given in b) and then the solution is zoomed in c). Figure 2 shows a similar comparison starting from the solution for $t = 1.6$ in Figure 10 for the Dam Break problem, then a solution in a four times coarser mesh and a zoomed area for the last solution are given (please check Sections 5.2 and 5.3 for a review of the Dam Break and Rayleigh-Taylor problems).

The physics of these two problems for the selected times have particular differences. In the Rayleigh-Taylor case, the problem is dominated by the falling of the more dense phase from top to bottom. Once the initial structures have been lost the flow continues as falling droplets which accumulates at the bottom of the domain. In the case of the Dam Break problem after the initial column has collapsed some droplets are ejected from the splashing waves; however, the more important particulate physics is given by the less dense phase trapped in the mixing process. These particles behave as bubbles which rise by buoyancy forces.

Since the interface is resolved in about two or three cells (Trontin et al., 2008) by the VOF method, a chunk (small fluid structure, see the structures
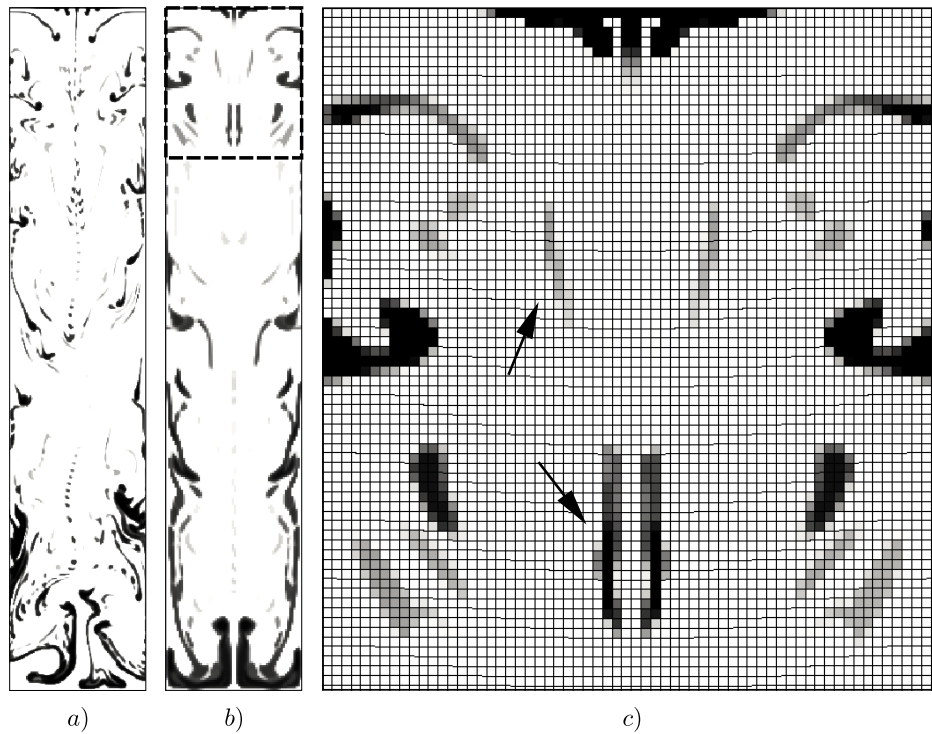
Figure 1: Results for the Rayleigh-Taylor problem for $t = 5.4$. a) results in fine mesh, b) results in coarse mesh, c) detail for the dashed line box in b) with superimposed mesh (grayscale saturated to black at $\alpha_q = 0.3$). Selected unresolved chunks are indicated by the arrows
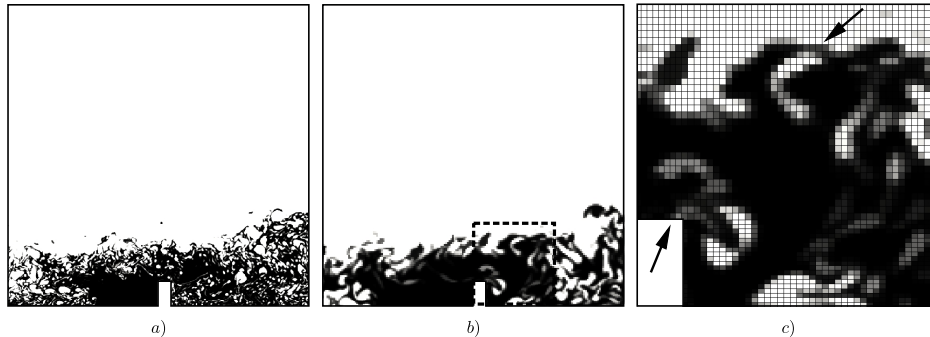
Figure 2: Results for the Dam Break problem for $t = 1.6$. a) results in fine mesh, b) results in coarse mesh, c) detail for the dashed line box in b) with superimposed mesh (grayscale saturated to black at $\alpha_q = 0.3$). Selected unresolved chunks are indicated by the arrows

marked by the arrows in the figures) needs around four to six cells in width to be correctly resolved. In the case of bubbles and droplets, they should have about ten cells in diameter for a correct curvature calculation. The practical consequence on these small structures is the wrong re-agrupation and break-up due to the surface tension terms since their effect is more numerical than physical (Rider and Kothe, 1998). In addition, the development of unresolved interface scale chunks has another important drawback: when the values of the volume fraction, α_q, of these chunks lay on intermediate values between 0 and 1 (grey zones in the figures) these structures loose their physical meaning. The fluid present within them is then treated as a new fluid with density and viscosity given by the value of the mixture properties. These properties do not match the values of none of the original two fluids and then the buoyancy forces and the drop falling will be incorrectly calculated.

The idea behind the model which will be presented is to treat the long scale structures of the flux purely with the VOF method. When some struc-

10

tures fall below the unresolved scale this zones have to be calculated using the ASMM using appropriate closure laws.

3. Theoretical foundation

3.1. The Algebraic Slip Mixture Model

The Algebraic Slip Mixture Model is a multi-phase model for n interpenetrated phases based on the Multi-fluid model (Ishii, 1975; Ishii and Hibiki, 2010). In this model all the phases are treated as a mixture which exhibits mean properties for density and viscosity. In the Multi-fluid, model a mass and a momentum equations are solved for each phase; on the other hand, the ASMM reduces the system to a mass and a momentum equations for the whole mixture and one mass conservation equation for each of the $n-1$ phases. Since the momentum equations for these $n-1$ phases are not solved, additional *algebraic* relationships for each phase velocities with respect to the mixture velocity are given. These algebraic relationships for the slip velocities give the name to this mixture model. Finally, a closure law for all phases volume fractions is also included. Even when ASMM is physically more limited than Multi-fluid model, its results are in some particular cases comparable to that model due to the lack of closure laws available for the Multi-fluid model (Manninen et al., 1996).

The Mixture Model can be formulated using either the so called *velocity of center-of-mass*, *mixture velocity* or *mass averaged velocity*, or in terms of the *velocity of center-of-volume*. Starting from the Multi-fluid method, the velocity of center-of-mass based formulation can be derived (Manninen et al., 1996), which is given by Eqn. (1)

$$
\begin{cases}
\frac{\partial}{\partial t}(\rho_m) + \vec{\nabla} \cdot (\rho_m \vec{v}_m) = 0 \\[3mm]
\frac{\partial}{\partial t}(\rho_m \vec{v}_m) + \vec{\nabla} \cdot (\rho_m \vec{v}_m \otimes \vec{v}_m) = -\vec{\nabla}p + \vec{\nabla} \cdot \left[\mu_m \left(\vec{\nabla} \vec{v}_m \right. \right. \\[3mm]
\left. \left. + \vec{\nabla} \vec{v}_m^{\mathrm{T}} \right) \right] + \rho_m \vec{g} - \vec{\nabla} \cdot \left[\rho_m c_p \left(1 - c_p \right) \vec{v}_{pq} \otimes \vec{v}_{pq} \right] \\[3mm]
\frac{\partial}{\partial t}(\alpha_p) + \vec{\nabla} \cdot (\alpha_p \vec{v}_m) = -\vec{\nabla} \cdot \left[\alpha_p \left(1 - c_p \right) \vec{v}_{pq} \right]
\end{cases}
\tag{1}
$$

where $\rho_m = \sum_{k=1}^n \alpha_k \rho_k$ is the mixture density; $\vec{v}_m = \frac{\sum_{k=1}^n \alpha_k \rho_k \vec{v}_k}{\rho_m}$ is the velocity of center-of-mass, which is calculated from the phase velocities $\vec{v}_k$, the fractions α_k (which obey the closure law $\sum_{k=1}^n \alpha_k = 1$) and the densities ρ_k; p is the pressure, which is common for all the phases; $\mu_m = \sum_{k=1}^n \alpha_k \mu_k$ is the dynamic viscosity of the mixture; $\vec{g}$ is the gravitational acceleration; $c_k = \frac{\alpha_k \rho_k}{\rho_m}$ is the mass fraction for the phase k and $\vec{v}_{pq} = \vec{v}_p - \vec{v}_q$ is the relative velocity for a given phase, p, with respect to another phase, q. This relative velocity can be calculated by algebraic expressions related to the physics of the dispersed phase. For the sake of simplicity, it is convenient to set a general constitutive law for the relative velocity, $\vec{v}_{pq}$, as it is shown in Eqn. (2)

$$
\vec{v}_{pq} = \vec{v}_{rc} \left(1 - \alpha_p \right)^a
\tag{2}
$$

where $\vec{v}_{rc}$ and a are constants for the model. The $\vec{v}_{rc}$ constant can be interpreted as the velocity of a single bubble or droplet moving in the continuum phase. This expression is flexible and allows to match several other models, for example the Schiller & Naumann drag law (Schiller and Naumann, 1935)

12

can be fitted by selecting an appropriate value for v_{rc} and with $0 \leqslant a \leqslant 1$. In addition, Ishii & Hibiki (Ishii and Hibiki, 2010) provide a complete reference for drag laws in several industrial cases. Finally, the momentum equation has an extra term accounting for the momentum exchanging between the phases, which is calculated by the drift tensor, $\overline{\overline{\tau_D}}$ in Eqn. (3)

$$\overline{\overline{\tau_D}} = \rho_m c_p \left(1 - c_p\right) \vec{v}_{pq} \otimes \vec{v}_{pq} \tag{3}$$

The resulting system is composed by the mass conservation equation for the mixture, the momentum equation for the mixture velocity and the mass conservation equation for the secondary phase p in a two-components mixture (p and q), where the p phase is the dispersed one. This system of three equations has three unknowns, which are: $\vec{v}_m$, p and α_p. Respect to ρ_m it is linked to α_p via its constitutive equation. As it is usual in incompressible problems the pressure has no evolution equation, so that it becomes a Lagrange multiplier for the restriction given by the mixture density transport equation. This characteristic leads to a pressure-velocity coupling that can be treated in several ways, as the Fractional-Step or PISO/SIMPLE like methods (Gastaldo et al., 2008) among others. This issue appears also in reacting flows (Babik et al., 2005; Najm et al., 1998; Knio et al., 1999), the Low-Mach solvers applied in that problems are also an inspiration for the solution of ASMM problems. In addition α_p has to be bounded in the [0, 1] interval to have physical meaning. Since v_m is not divergence free and that the momentum and mixture conservation equations depend on α_p the boundedness is not a direct consequence of the correct discretization of the third equation in Eqn. (1), but of the whole system (Gastaldo et al., 2011).

13

As was stated previously, another formulation can be devised for ASMM in terms of the velocity of the center-of-volume or the *volumetric flux*. To do so it is necessary to find a relationship between the velocity of center-of-mass and this new velocity (Bohorquez, 2012; Márquez Damián, 2013). The desired relationship is shown in Eqn. (4)

$$\vec{v}_m = \vec{u} + \alpha_q \left(1 - \alpha_q\right) \frac{\rho_q - \rho_p}{\rho_m} \vec{v}_{qp} \tag{4}$$

Now, starting from the Multi-fluid method it is possible to find a new mass conservation equation for the mixture written in terms of the velocity of center-of-volume. Then, for a given phase k of the system the mass conservation equation (without sources) reads as in Eqn. (5)

$$\frac{\partial \alpha_k \rho_k}{\partial t} + \vec{\nabla} \cdot (\alpha_k \rho_k \vec{v}_k) = 0 \tag{5}$$

assuming constant densities for all phases, dividing each mass conservation by its corresponding density and then summing over all phases and recalling that $\sum_{k=1}^{n} \alpha_k = 1$, the final expression is given by Eqn. (6)

$$\vec{\nabla} \cdot \vec{u} = 0 \tag{6}$$

where $\vec{u} = \sum_{k=1}^{n} \alpha_k \vec{v}_k$ is the velocity of center-of-volume. Now, taking a biphasic system, the mass conservation equation for the primary (continuum) phase can be obtained and the relationship given in Eqn. (7) can be derived,

$$\vec{v}_q = \vec{u} + \left(1 - \alpha_q\right) \vec{v}_{qp} \tag{7}$$

Replacing this expression in Eqn. (5) for the q phase allows to write the final expression for the mass conservation equation for the q phase, Eqn. (8),

14

$$\frac{\partial \alpha_q}{\partial t} + \vec{\nabla} \cdot (\alpha_q \vec{u}) + \vec{\nabla} \cdot [\alpha_q (1 - \alpha_q) \, \vec{v}_{qp}] = 0 \tag{8}$$

Finally, the mixture momentum equation can be rewritten in terms of the primary phase void fraction α_q and the relative velocity of the primary phase with respect to the secondary one $\vec{v}_{qp}$. Starting from the expression of the drift tensor in Eqn. (3), taking into account that $\vec{v}_{qp} = -\vec{v}_{pq}$ and $\alpha_q = 1 - \alpha_p$ and doing some algebraic simplifications, it becomes which is shown in Eqn. (9)

$$\overline{\overline{\tau_{\mathrm{D}}}} = \rho_m c_p (1 - c_p) \, \vec{v}_{pq} \otimes \vec{v}_{pq} = \alpha_q \, (1 - \alpha_q) \, \frac{\rho_q \, \rho_p}{\rho_m} \vec{v}_{qp} \otimes \vec{v}_{qp} \tag{9}$$

In order to give stability to the solution and to simplify the definition of the boundary conditions (Berberovic et al., 2009) the treatment of the pressure terms can be performed using the modified pressure p_{rgh} defined in Eqn. (10)

$$p_{rgh} = p - \rho_m \vec{g} \cdot \vec{x} \tag{10}$$

where $\vec{x}$ is the position vector. Thus, the pressure gradient is then expressed as in Eqn. (11)

$$-\vec{\nabla} p = -\vec{\nabla} p_{rgh} - \vec{g} \cdot \vec{x} \vec{\nabla} \rho_m - \rho_m \, \vec{g} \tag{11}$$

regrouping terms the Eqn. (12) is obtained

$$-\vec{\nabla} p + \rho_m \, \vec{g} = -\vec{\nabla} p_{rgh} - \vec{g} \cdot \vec{x} \vec{\nabla} \rho_m \tag{12}$$

15

which allows to replace the pressure gradient and gravity terms in the second equation of Eqn. (13) by a function of the modified pressure.

In summary, the continuity equation and the momentum balance for the mixture and the mass conservation equation for the primary phase in center-of-volume based formulation may be written as in Eqn. (13)

$$
\begin{cases}
\vec{\nabla} \cdot \vec{u} = 0 \\[2ex]
\frac{\partial}{\partial t}(\rho_m \vec{v}_m) + \vec{\nabla} \cdot (\rho_m \vec{v}_m \otimes \vec{v}_m) = -\vec{\nabla} p_{rgh} \\[2ex]
\qquad + \vec{\nabla} \cdot \left[\mu_m \left(\vec{\nabla}\vec{v}_m + \vec{\nabla}\vec{v}_m^{\mathrm{T}} \right) \right] - \vec{g} \cdot \vec{x} \vec{\nabla}\rho_m \\[2ex]
\qquad\qquad - \vec{\nabla} \cdot \left[\alpha_q \left(1 - \alpha_q \right) \frac{\rho_q\, \rho_p}{\rho_m} \vec{v}_{qp} \otimes \vec{v}_{qp} \right] \\[2ex]
\frac{\partial \alpha_q}{\partial t} + \vec{\nabla} \cdot (\alpha_q \vec{u}) + \vec{\nabla} \cdot \left[\alpha_q \left(1 - \alpha_q \right) \vec{v}_{qp} \right] = 0
\end{cases}
\tag{13}
$$

This formulation is often called the Drift-Flux Model (Manninen et al., 1996) because it relies in the calculation of fluxes (center-of-volume velocities) instead of velocities (center-of-mass velocities) in the mass conservation equation of the primary phase. The principal advantage of this method is the possibility to use a divergence free velocity in the mass conservation equation for the primary phase. In addition, it is then possible to avoid solving a mass conservation equation for ρ_m which is no more an unknown but a derived quantity from ρ_q, ρ_p and α_q. On the other hand, this system has a mixed formulation between center-of-volume and center-of-mass velocities which requires transformation formulas in order to solve the momentum

16

equation and perform the PISO loop, these formulas are based in Eqn. (4).

3.2. The Volume of Fluid method as a Mixture Model

The VOF method can be classified as a interface capturing technique which implies that the free-surface is not exactly tracked by the mesh like in interface tracking methods, but its position is approximated by a phase fraction function (Carrica et al., 2006). In this sense, the phase fraction function plays the same role as in ASMM. This similarity can be exploited in view of the unified framework needed for an extended mixture model.

So that, it would be valuable to find a derivation of the VOF method from the ASMM. This sets a difference with respect to the original approach given by Hirt & Nichols (Hirt and Nichols, 1981) in the presentation of the method. This derivation allows to understand the similarities between both methods and the potential for an unified framework and solver. The derivation of the VOF method starts recalling the center-of-volume formulation of the ASMM, as is presented in Eqn. (13). A principal difference between ASMM and the VOF method is that the VOF method considers a continuous velocity field along all the interfaces, which is consistent with the interface boundary conditions given by the physics of fluids. This is possible since all the interfaces are supposed to be resolved at DNS scale. This hypothesis implies that the relative velocity between phases is null, $\vec{v}_{qp} = 0$. Thus, recalling the relationship between the center-of-mass velocity, $\vec{v}_m$ and the center-of-volume velocity, $\vec{u}$ given by Eqn. (4) the result is given by Eqn. (14)

17

$$\vec{v}_m = \vec{u} + \alpha_q \left(1 - \alpha_q\right) \frac{\rho_q - \rho_p}{\rho_m} \vec{v}_{qp} =$$

$$(14)$$

$$\vec{u} + \alpha_q \left(1 - \alpha_q\right) \frac{\rho_q - \rho_p}{\rho_m} 0 = \vec{u}$$

which implies that the velocity of center-of-mass and the velocity of center-of-volume are equivalent. By inspection of the momentum equation given in the system of Eqn. (13) it is clear that the drift tensor $\overline{\overline{\tau_D}} = \alpha_q \left(1 - \alpha_q\right) \frac{\rho_q \rho_p}{\rho_m} \vec{v}_{qp} \otimes \vec{v}_{qp}$ is null. In addition, the possibility of capturing long-scale interfaces allows to model the effects of the surface tension. This effect is modeled by the Continuum Surface Model (CSF) (Brackbill et al., 1992) which adds to the momentum equation the term given in Eqn. (15)

$$\vec{F}_\sigma = \sigma \kappa \vec{\nabla} \alpha_q \qquad (15)$$

where κ is the mean curvature of the free surface which is given by Eqn. (16)

$$\kappa = \vec{\nabla} \cdot \left(\frac{\vec{\nabla} \alpha_q}{\left| \vec{\nabla} \alpha_q \right|} \right) \qquad (16)$$

Finally it is important to note that the third equation of Eqn. (13) can be also simplified since the nonlinear term is zero due to the null relative velocity $\vec{v}_{qp}$. This term is deliberately included in the formulation with the aim to compress the interface. It is worthy to note that since in VOF method α_q is expected to be ever valued 0 or 1, except for the interfaces, this term acts only on this place (Berberovic et al., 2009; Rusche, 2002; OpenCFD, 2005; Weller, 2008) and vanishes otherwise, so the original formulation for VOF is recalled in general and the non-linear term is used only at interface zones. Thus, the solved system reads as in Eqn. (17)

18

$$
\begin{cases}
\vec{\nabla} \cdot \vec{u} = 0 \\
\\
\frac{\partial}{\partial t}(\rho_m \vec{u}) + \vec{\nabla} \cdot (\rho_m \vec{u} \otimes \vec{u}) = -\vec{\nabla} p_{rgh} \\
\\
+\vec{\nabla} \cdot \left[\mu_m \left(\vec{\nabla} \vec{u} + \vec{\nabla} \vec{u}^{\mathrm{T}} \right) \right] - \vec{g} \cdot \vec{x} \vec{\nabla} \rho_m + \sigma \kappa \vec{\nabla} \alpha_q \\
\\
\frac{\partial \alpha_q}{\partial t} + \vec{\nabla} \cdot (\alpha_q \vec{u}) + \vec{\nabla} \cdot \left[\alpha_q \left(1 - \alpha_q \right) \vec{v}_{qp} \right] = 0
\end{cases}
\tag{17}
$$

This formulation will hereinafter referred as the Weller-VOF method.

3.3. A coupled model

From the comparison of the systems given in Eqn. (13) and Eqn. (17), it becomes clear that both VOF and ASMM models can be written in a very close formulation, and even more, the VOF model can be directly derived from the ASMM. The basic differences between these approaches in the context of the mixture models are the terms related to the different scales. So that, since the interfaces are supposed to be completely captured, the VOF model has a term in the momentum equation including the effects of the surface tension. On the other hand, the ASMM does not include this term; however, it takes into account the effect of the drift stresses, or the effect of the small scale interfaces. In addition, the relative velocity between phases has physical meaning in ASMM while in VOF it is only a numerical tool in order to compress the interface. So that, using θ as a flag to activate or deactivate certain terms according to the interface scale which is being resolved, VOF (Weller-VOF) and ASMM can be coupled as in Eqn. (18)

19

$$
\begin{cases}
\vec{\nabla} \cdot \vec{u} = 0 \\[2em]
\frac{\partial}{\partial t}\left(\rho_m \vec{v}_m\right) + \vec{\nabla} \cdot \left(\rho_m \vec{v}_m \otimes \vec{v}_m\right) = -\vec{\nabla} p_{rgh} \\[2em]
+ \vec{\nabla} \cdot \left[\mu_m \left(\vec{\nabla}\vec{v}_m + \vec{\nabla}\vec{v}_m^{\mathrm{T}}\right)\right] - \vec{g} \cdot \vec{x}\vec{\nabla}\rho_m + \theta\,\sigma\kappa\vec{\nabla}\alpha_q \\[2em]
- \left(1 - \theta\right) \vec{\nabla} \cdot \left[\alpha_q \left(1 - \alpha_q\right) \frac{\rho_q\,\rho_p}{\rho_m}\vec{v}_{qp} \otimes \vec{v}_{qp}\right] \\[2em]
\frac{\partial \alpha_q}{\partial t} + \vec{\nabla} \cdot \left(\alpha_q \vec{u}\right) + \vec{\nabla} \cdot \left\{\alpha_q \left(1 - \alpha_q\right)\left[\theta\,\vec{v}_{qp,\mathrm{VOF}}\right.\right. \\[2em]
\left.\left.+ \left(1 - \theta\right)\vec{v}_{qp,\mathrm{ASMM}}\right]\right\} = 0
\end{cases}
\tag{18}
$$

where $\vec{v}_{qp,\mathrm{VOF}}$ and $\vec{v}_{qp,\mathrm{ASMM}}$ are the relative velocities calculated either numerically or physically. The value of θ coefficient is $\theta = 1$ for VOF and $\theta = 0$ for ASMM. Two methodologies to calculate θ are studied, in order to select the most convenient for the proposed algorithm.

3.3.1. Černe criterion

One of the available criteria for long and short scale models coupling, used by several authors, was given by Cerne (Černe et al., 2001). It is based on the analysis of the frame obtained taking into account a given cell and all it neighbors by faces and edges, as it is shown in Figure 3. The switching function γ is obtained finding the minimum of the function G as is shown in Eqns. (19-20)
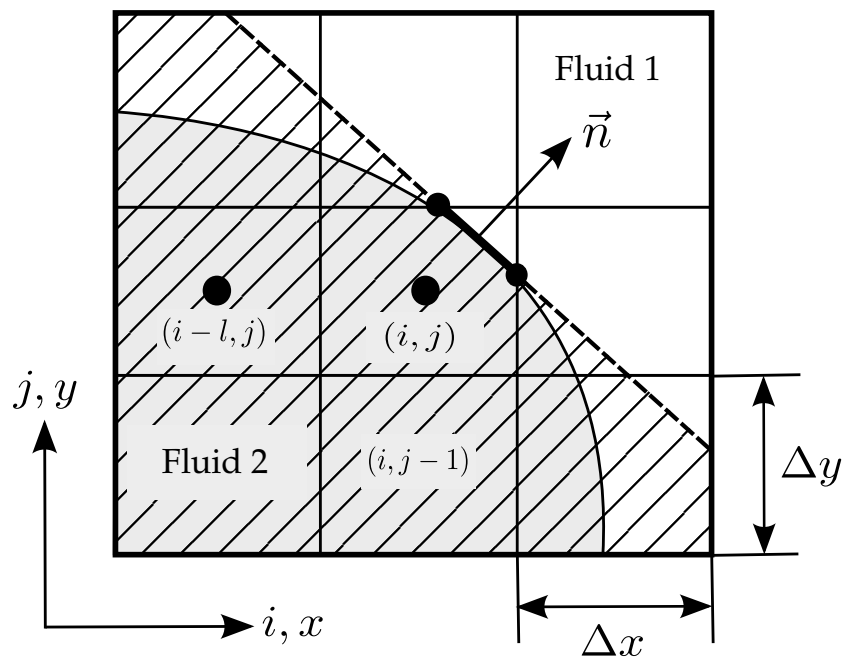
20

Figure 3: Interface reconstruction using the Cerne criterion (Adapted from (Černe et al., 2001))

$$G_{i,j}\left(\vec{n}\right) = \sum_{l=-1}^{1} \sum_{k=-1}^{1} \left(\alpha_{q,i+k,j+l} - \alpha'_{q,i+k,j+l}\left(\vec{n}\right)\right)^2 \tag{19}$$

$$\gamma_{i,j} = \min\left(G_{i,j}\left(\vec{n}\right)\right) \tag{20}$$

where α'_q represents the volume fraction of the hatched area. The minimum value of γ is zero and corresponds to the exact matching of the interface with the boundary of the hatched zone. This value increases when the fluid is located in the wrong side of the proposed interface, so that this function is often called the "dispersion function". Finally, it is necessary to set a threshold value for $\gamma = \gamma_0$ such that the θ criterion could be calculated as in Eqn. (21)

$$\theta = \begin{cases} 1, \text{ if } \gamma_{i,j} < \gamma_0 & [\text{VOF in cell}\,(i,j)] \\ \\ 0, \text{ if } \gamma_{i,j} > \gamma_0 & [\text{Multi} - \text{fluid in cell}\,(i,j)] \end{cases} \tag{21}$$

The threshold value is obtained by several cases study, such that the recommended value is $\gamma_0 \cong 0.6$ (Černe et al., 2001). This methodology is attractive since it is based in the reconstruction of the interface (Puckett et al., 1997), but requires the time consuming solution of a minimization problem at each cell and time-step.

3.3.2. Face gradient criterion

Another criterion can be devised based on the gradient of the phase fraction function α_q calculated by the cell-centered Finite Volume Method (FVM) (Jasak, 1996; Márquez Damián, 2013), which is shown in Eqn. (22)

$$\vec{\nabla}\alpha = \frac{1}{V}\sum_f (\alpha_q)_f \cdot \vec{S}_f \tag{22}$$

where V is the volume of a given cell, f is an index along all the faces of the cell and $\vec{S}_f$ is the face area vector. As a next step, this gradient is interpolated at faces obtaining $\vec{\nabla}\alpha_f$. The gradient at the faces gives a general idea of the variation of the phase fraction along the domain. Large gradients are associated to big changes in α, and then a large scale interface is inferred. This value is weighted with a measure of the mesh in order to normalize the switching function. A clear local jump between two phases requires not only a big gradient but also to be extended in few cells. So that, the gradient is multiplied by the face's neighboring cells center-to-center vector, $\vec{d}_{PN}$ as is shown in Eqns. (23)-(24) (See Figure 4)

$$\vec{d}_{PN} = \vec{x}_P - \vec{x}_N; \tag{23}$$

$$\gamma_f = |\vec{\nabla}\alpha_f \cdot \vec{d}_{PN}| \tag{24}$$

Finally, the criterion to switch between VOF and ASMM is given by the rules expressed in Eqn. (25). It states that VOF will be used in high relative gradient zones (large scale interfaces) and in regions with $\alpha \cong 1$ or $\alpha \cong 1$, indicating pure phases; in all other cases, ASMM will be used. This criterion requires the selection of γ_0, the threshold for small gradients and ϵ, which is a magnitude that controls the maximum deviation from $\alpha = 1$ or $\alpha = 0$ to be considered as a pure phase.
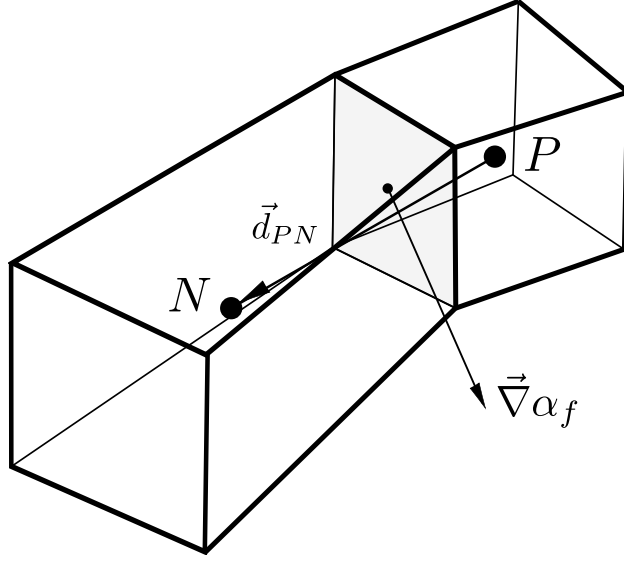
Figure 4: Face gradient criterion

$$\theta_f = \begin{cases} 1, \text{ if } \alpha_f < 0 + \epsilon \text{ o } \alpha_f > 1 - \epsilon & [\text{VOF in face } f] \\ \\ 1, \text{ if } \gamma_f > \gamma_0 & [\text{VOF in face } f] \\ \\ 0, \text{ if } \gamma_f < \gamma_0 & [\text{ASMM in face } f] \end{cases} \quad (25)$$

The values for γ_0 and ϵ have to be adjusted according to the problem. Since in VOF the interface is resolved in about three cells a reference value is $\gamma_0 = 0.33$. Respect to ϵ, a typical value is $\epsilon = 5 \times 10^{-3}$. The principal advantages of this indicator function are its intrinsic 3D formulation and its simplicity and low demanding calculation. This method will be then used for model switching.

4. Solver implementation

The implementation of the solver for the coupled model or extended mixture model given by Eqn. (18) is based on the FVM using the OpenFOAM® libraries (Weller et al., 1998). The starting point is the discretization of the Navier-Stokes system, which is presented in Eqn. (26)

$$
\begin{cases}
\frac{\partial \vec{v}}{\partial t} + \vec{\nabla} \cdot (\vec{v} \otimes \vec{v}) = -\vec{\nabla} p + \vec{\nabla} \cdot \left(\nu \vec{\nabla} \vec{v} \right) \\[2em]
\vec{\nabla} \cdot \vec{v} = 0
\end{cases}
\tag{26}
$$

here, the momentum equation is presented with the continuity equation which corresponds to the case of constant density in space and time, thus, it is a case of incompressible flow. This system deals with three principal issues: first, the incompressibility which leads to a lack of pressure evolution equation and requires an special treatment for pressure-velocity coupling; the left two other issues are related to the convective term which requires stabilization for the advection and a particular treatment of its non-linearity. The stabilization is treated by High Resolution Methods as is usual in the FVM (Hirsch, 2007). With respect to the non-linearity, it can be solved by using a non-linear system or by linearization which is the chosen option. So that, the advective term is linearized using the assumption of small Courant numbers ($\mathbf{Co} < 1$) and then $\vec{v}^0 \cong \vec{v}$, as is presented in Eqn. (27)

25

$$\int_\Gamma \vec{\nabla} \cdot (\vec{v} \otimes \vec{v}^0) \cdot d\vec{\Gamma} = \sum_f \vec{v}_f \, \vec{v}_f^0 \cdot \vec{S}_f$$

$$= \sum_f F^0 \, \vec{v}_f \tag{27}$$

$$= a_P \vec{v} + \sum_f a_N \vec{v}_N$$

where $\vec{v}^0$ is the velocity at the previous time-step, a_P are the diagonal coefficients of the discretization matrix, a_N the off-diagonal ones and F^0 the face flux at the previous time-step. All these quantities are a function of $\vec{v}^0$, it is important to note that the pressure is discretized at cell centres and the velocities are calculated at faces in the form of fluxes, so that the flux F^0 is only calculated from $\vec{v}^0$ eventually at the first time-step. In the rest of the simulation this flux is taken from the previous time-step pressure-velocity loop, which assures the satisfaction of the continuity equation (conservative flux). Regarding the incompressibility restriction it is treated in this work by the PISO (Pressure Implicit Split of Operators) procedure (Issa, 1986), as is implemented in OpenFOAM® (Jasak, 1996; Peng Karrholm, 2008).

4.1. Derivation of an equation for the pressure

Since no evolution equation is given for the pressure it is necessary to derive a method to obtain at least a discretized equation which allow to solve the pressure. Writing the momentum equation in a semi-discretized form as in Eqn. (28) it is possible to start its derivation

$$a_P \vec{v}_P = \vec{H}(\vec{v}) - \vec{\nabla} p \tag{28}$$

26

This equation is obtained by the integral form of the momentum equation using the FVM. The pressure gradient is not discretized at this time, which following the Rhie and Chow interpolation procedure (Rhie and Chow, 1983). It is important to note that in order to allow future face interpolations of matrix's coefficients, the discretization has been divided by the volume of each cell.

The $\vec{H}(\vec{v})$ operator accounts for the advective and diffusive terms, as well as all the source terms, including the source part of the transient term, so that it results to be which is shown in Eqn. (29)

$$\vec{H}(\vec{v}) = -\sum_f a_N \vec{v}_N + \frac{\vec{v}^0}{\Delta t} \tag{29}$$

Then, the velocity at cell-centers can be isolated from the discretized version of momentum equation [Eqn. (28)] as in Eqn. (30)

$$\vec{v}_P = \frac{\vec{H}(\vec{v})}{a_P} - \frac{1}{a_P}\vec{\nabla}p \tag{30}$$

In addition these velocities can be interpolated at faces as in Eqn. (31):

$$\vec{v}_f = \left(\frac{\vec{H}(\vec{v})}{a_P}\right)_f - \left(\frac{1}{a_P}\right)_f \left(\vec{\nabla}p\right)_f \tag{31}$$

which gives a base for face flux calculation. On the other hand, the continuity equation can be discretized as in Eqn. (32)

$$\vec{\nabla} \cdot \vec{v} = \sum_f \vec{v}_f \cdot \vec{S}_f = 0 \tag{32}$$

Now, the obtained expression for the velocity at faces can be substituted in Eqn. (32) to find an equation for the pressure [Eqn. (33)]

$$\vec{\nabla} \cdot \left(\frac{1}{a_P} \vec{\nabla} p \right) = \vec{\nabla} \cdot \left(\frac{\vec{H}(\vec{v})}{a_P} \right) \tag{33}$$

Finally, the new set of discrete equations for the Navier-Stokes system results to be which is shown in Eqn. (34)

$$\begin{cases} a_P \vec{v}_P = \vec{H}(\vec{v}) - \vec{\nabla} p \\ \sum_f \left[\left(\frac{1}{a_P} \right)_f \left(\vec{\nabla} p \right)_f \right] \cdot \vec{S}_f = \sum_f \left(\frac{\vec{H}(\vec{v})}{a_P} \right)_f \cdot \vec{S}_f \end{cases} \tag{34}$$

In addition, it is necessary a way to assemble the face flux F, see Eqn. (35)

$$F = \vec{v}_f \cdot \vec{S}_f = \left[\left(\frac{\vec{H}(\vec{v})}{a_P} \right)_f - \left(\frac{1}{a_P} \right)_f \left(\vec{\nabla} p \right)_f \right] \cdot \vec{S}_f \tag{35}$$

4.2. A PISO solver for the Extended Model

The derivation of a solver for the Extended Model is based on the solver for the Weller-VOF method given in the OpenFOAM® suite, which is called `interFoam`. It relies on a pressure-velocity coupling loop based on PISO, and is basically a derivation of the method presented in the previous section. In addition it is necessary to solve the α_q equation which is achieved by means of the Multidimensional Universal Limiter for Explicit Solution (MULES) an explicit solver based on the Flux Corrected Transport (FCT) technique (Zalesak, 1979; Rudman, 1997; Márquez Damián, 2013). The use of the MULES integrator gives a bounded value for α_q^{n+1} and returns a limited version of the flux used in the integration, which is needed to assemble the momentum equation.

So that, the general method for the solution of α_q equation is based in its discretized form given in Eqn. (36)

$$\frac{\partial \alpha_q}{\partial t} + \vec{\nabla} \cdot (\alpha_q \vec{u}) + \vec{\nabla} \cdot \{\alpha_q (1 - \alpha_q) [\theta \, \vec{v}_{qp,\text{VOF}}$$

(36)

$$+ (1 - \theta) \, \vec{v}_{qp,\text{ASMM}}]\} = 0$$

This equation can be rewritten in terms of face fluxes and using an explicit integration scheme as in Eqn. (37)

$$\frac{\alpha_q^{n+\nu+1} - \alpha_q^n}{\Delta t} V + \sum_f F_{\alpha_q} =$$

$$\frac{\alpha_q^{n+\nu+1} - \alpha_q^n}{\Delta t} V + \sum_f \left\{ \left(\alpha_q^{n+\nu} \right)_f F^{n+\nu} \right.$$

(37)

$$\left. + \left[\alpha_q^{n+\nu} \left(1 - \alpha_q^{n+\nu} \right) \right]_f F^{NL,n+\nu} \right\} = 0$$

where F_{α_q} represents the whole flux of the α_q equation. This equation is solved using a fixed-point iteration in order to circumvent the issue of the non-linearity of the fluxes, where ν is the number of the present iteration. The loop is done `nAlphaCorrectors` times. The flux F_{α_q} is calculated from $F^n = \vec{u}_f \cdot \vec{S}_f$ which is a linear flux due to the center-of-volume velocity and $F^{NL,n}$, the non-linear flux due to the combination of the artificial compressive velocity and the physical relative velocity at the interfaces. This is calculated as in Eqn. (38)

$$F^{NL,n} = \left[(1 - \theta_f) \, \vec{v}_{rc} \left(\alpha_q^n \right)^a \right]_f \cdot \vec{S}_f$$

(38)

$$+ \theta_f \, n_f \min \left[C_\alpha \frac{|F^n|}{|\vec{S}_f|}, \max \left(\frac{|F^n|}{|\vec{S}_f|} \right) \right]$$

where the first term corresponds to the flux due to the physical relative velocity calculated by Eqn. (2), and the second one corresponds to the effect

29

of the artificial compressive velocity. There, C_α (`cAlpha`) is an adjustment constant, $n_f = \frac{(\nabla \alpha_q)_f}{\left|(\nabla \alpha_q)_f + \delta_n\right|} \cdot \vec{S}_f$ is the face unit normal flux with $\delta_n = \frac{\varepsilon}{\left(\frac{\sum_N V_i}{N}\right)^{1/3}}$ as a stabilization factor to avoid division by zero, with $\varepsilon = 1 \times 10^{-8}$. The direction of the compressive velocity is given by the gradient of α_q and ensures the application of the compression on the normal of the interface. The values of $\left(\alpha_q^n\right)_f$ are calculated by a selectable High Resolution Scheme, particularly in the non-linear term they can be discretized by the *interfaceCompression* scheme, which has been devised specially for its use in equation (37). This scheme doesn't obey to an TVD/NVD analysis; however it was selected in order to guarantee the use of upwind differencing when α_q is near the extrema, or central differencing otherwise being a good combination of boundedness and accuracy (Peng Karrholm, 2008; Weller, 2008) (see (Gastaldo et al., 2011) for an example of this kind of method in ASMM solving under a different solution methodology). Once the flux F_{α_q} is assembled it is used by MULES to perform the integration given by Eqn. (36). Here it is important to note that MULES use a limited version of F_{α_q} in the integration which is then returned with the new value of α_q for further use.

In addition, the solution method of the system given in Eqn. (17) includes an adaptive time-step control and the sub-cycling in the solution of α_q equation. The adaptive time-step control is performed calculating the time-step by means of Eqn. (39)

$$\Delta t^n =$$

$$\min \left\{ \frac{\mathbf{Co}_{max}}{\mathbf{Co}} \Delta t^0, \left(1 + \lambda_1 \frac{\mathbf{Co}_{max}}{\mathbf{Co}}\right) \Delta t^0, \lambda_2 \Delta t^0, \Delta t_{max} \right\} \tag{39}$$

where $\mathbf{Co} = \frac{|\vec{u}_f \cdot \vec{S}_f|}{\vec{d}_{PN} \cdot \vec{S}_f} \Delta t$ is the face-calculated Courant number, $\mathbf{Co}_{max}$, Δt_{max} are user-defined parameters and $\lambda_1 = 0.1$ and $\lambda_2 = 1.2$ are two hard-coded factors in order to reduce immediately the time-step and to increase it gradually to avoid unstable oscillations. Regarding to $\mathbf{Co}_{max}$, Gopala and van Wachem (Gopala and van Wachem, 2008) recommend a value lesser than 0.3 and Berberovic *et al.* (Berberovic et al., 2009) a value of approximately 0.2. By the author's experience, the last value results successful, but some runnings have been performed using $\mathbf{Co}_{max} = 0.1$ to reach the expected results. It is important to note another observed behavior of the adaptive time-step method. Since it is Courant number based, the time-step can go to excessive high values at the beginning of the simulation if no high velocity values are present in the simulated problem, which can can play against the physics of the phenomenon giving inaccurate values. This issue can be circumvented using the Δt_{max} parameter or using a fixed time-step in the first steps. Similar conclusions were informed by Berberovic *et al.*

The sub-cycling is performed in order to give stability to the solution of the α_q equation, so that choosing a number of sub-cycles n_{sc} (`nAlphaSubCycles`) the sub-step is defined as in Eqn. (40)

$$\Delta t_{sc} = \frac{\Delta t}{n_{sc}} \tag{40}$$

Since the flux used in the integration of the α_q equation is based on a center-of-volume velocity, it is necessary to give a center-of-mass velocity flux of mass flux in order to be able to assemble the momentum equation. This mass flux has to be calculated carefully within each sub-cycle. The basic assembling of this flux is given by the relationship between the center-of-

31

mass velocity and the center-of-volume velocity and is necessary since the α_q equation modifies the mass distribution, so that recalling Eqn. (4) and assembling a mass face flux, it becomes as is shown in Eqn. (41)

$$F_{\rho m} = (\rho_m \vec{v}_m)_f \cdot \vec{S}_f = (\rho_m \vec{u})_f \cdot \vec{S}_f$$

$$+ \left[\alpha_q \left(1 - \alpha_q \right) \left(\rho_q - \rho_p \right) \vec{v}_{qp} \right]_f \cdot \vec{S}_f$$

(41)

which can be re-written as in Eqn. (42)

$$F_{\rho m} = \rho_m \, F + \alpha_q \left(1 - \alpha_q \right) \left(\rho_q - \rho_p \right) F^{NL} \tag{42}$$

where F^{NL} is the face flux given by Eqn. (38). On the other hand the discretization of α_q requires the assembling of the flux given in Eqn. (43) [see Eqn. (37)]

$$\mathrm{F}_{\alpha_q} = (\alpha_q)_f \, F + \left[\alpha_q \left(1 - \alpha_q \right) \right]_f F^{NL} \tag{43}$$

Now, doing some simple algebraic manipulations, it is easy to reach what is shown in Eqn. (44)

$$F_{\rho m, sc, i} = \mathrm{F}_{\alpha_q} \left(\rho_q - \rho_p \right) + F \, \rho_p \tag{44}$$

So that, in each sub-cycle a partial mass flux is assembled as $F_{\rho m, sc, i}$. The mass flux for the complete time-step is obtained by the discrete integral form of the mean value theorem as in Eqn. (45)

$$F_{\rho m} = \sum_{i=1}^{n_{sc}} \frac{\Delta t_{sc}}{\Delta t} F_{\rho m, sc, i} \tag{45}$$

Once the α_q is solved it is necessary to assemble and solve the discretized version of the momentum equation in order to obtain a prediction of the center-of-mass velocity; this step is called the momentum predictor (`momentumPredictor`). This equation is shown in Eqn. (46)

$$\frac{\rho_m^{n+1}\tilde{\vec{v}}_m - \rho_m^n \vec{v}_m^n}{\Delta t} V + \sum_f F_{\rho_m}^{n+1} \, \vec{v}_m \cdot \vec{S}_f =$$

$$\sum_f \left(\mu_m^{n+1}\right)_f \left(\vec{\nabla}\vec{v}_m\right)_f \cdot \vec{S}_f + \left(\vec{\nabla}\vec{v}_m^n \cdot \vec{\nabla}\mu_m^{n+1}\right) V$$

$$-\sum_f \left(1 - \theta_f\right) \left[\alpha_q^{n+1}\left(1 - \alpha_q^{n+1}\right)\frac{\rho_q \, \rho_p}{\rho_m^{n+1}}\vec{v}_{qp}^n \otimes \vec{v}_{qp}^n\right]_f \cdot \vec{S}_f \qquad (46)$$

$$+\mathcal{R}\left\{\theta_f \left(\sigma\kappa\right)_f \left(\vec{\nabla}\alpha_q^{n+1}\right)_f\right.$$

$$\left.-\left[(\vec{g}\cdot\vec{x})_f \left(\vec{\nabla}\rho_m^{n+1}\right)_f - \left(\vec{\nabla}p_{rgh}^n\right)_f\right]\left|\vec{S}_f\right|\right\}$$

where F_{ρ_m} is the mass face flux given by $F_{\rho_m} = (\rho_m \vec{v}_m)_f \cdot \vec{S}_f$ and $\vec{a} = \mathcal{R}\left(\vec{a}\cdot\vec{S}_f\right)$ is an operator to reconstruct cell-centered fields from fields given as fluxes at faces.

In order to be able to obtain a PISO loop for the correction of the predicted center-of-mass velocity and the calculation of the modified pressure p_{rgh} it is necessary to have a flux relationship between the velocity of center-of-mass and the velocity of center-of-volume and to define a pressure equation. So that, starting from Eqn. (4), isolating $\vec{u}$ and multiplying by the face area vector the desired flux relationship is obtained in Eqn. (47)

33

$$F = \vec{u}_f \cdot \vec{S}_f = (\vec{v}_m)_f \cdot \vec{S}_f - \left[\alpha_q \left(1 - \alpha_q \right) \frac{\rho_q - \rho_p}{\rho_m} \right]_f (\vec{v}_{qp})_f \cdot \vec{S}_f \qquad (47)$$

From the derivation of the pressure equation in section 4.1 [Eqn. (31)] the velocity of center-of-mass can be expressed at faces (in terms of the modified pressure here) as in Eqn. (48)

$$(\vec{v}_m)_f = \left(\frac{\vec{H}(\vec{v}_m)}{a_P} \right)_f - \left(\frac{1}{a_P} \right)_f \left(\vec{\nabla} p_{rgh} \right)_f \qquad (48)$$

then, the flux relationship can be re-written as in Eqn. (49)

$$\vec{u}_f \cdot \vec{S}_f = \left[\left(\frac{\vec{H}(\vec{v_m})}{a_P} \right)_f - \left(\frac{1}{a_P} \right)_f \left(\vec{\nabla} p_{rgh} \right)_f \right] \cdot \vec{S}_f$$
$$- \left[\alpha_q \left(1 - \alpha_q \right) \frac{\rho_q - \rho_p}{\rho_m} \right]_f (\vec{v}_{qp})_f \cdot \vec{S}_f \qquad (49)$$

Using this expression in the discretized version of the incompressibility restriction for $\vec{u}$, $\sum_f \vec{u}_f \cdot \vec{S}_f = 0$ and re-arranging, Eqn. (50) is obtained

$$\sum_f \left[\left(\frac{1}{a_P} \right)_f \left(\vec{\nabla} p_{rgh}^{\nu+1} \right)_f \right] \cdot \vec{S}_f = \sum_f \left(\frac{\vec{H}(\vec{v_m})}{a_P} \right)_f \cdot \vec{S}_f$$
$$- \sum_f \left[\alpha_q \left(1 - \alpha_q \right) \frac{\rho_q - \rho_p}{\rho_m} \right]_f (\vec{v}_{qp})_f \cdot \vec{S}_f \qquad (50)$$

Finally, adding the effect of the gravitational acceleration and the surface tension, the pressure equation is obtained in Eqn. (51)

$$\sum_f \left[\left(\tfrac{1}{a_P} \right)_f \left(\vec{\nabla} p_{rgh}^{\nu+1} \right)_f \right] \cdot \vec{S}_f = \sum_f \left[\left(\tfrac{\vec{H}(\vec{v_m})}{a_P} \right)_f \right.$$

$$\left. + \theta_f \, (\sigma \kappa)_f \left(\vec{\nabla} \alpha_q^{n+1} \right)_f - (\vec{g} \cdot \vec{x})_f \left(\vec{\nabla} \rho_m^{n+1} \right)_f \right] \cdot \vec{S}_f \qquad (51)$$

$$- \sum_f \left[\alpha_q \, (1 - \alpha_q) \, \tfrac{\rho_q - \rho_p}{\rho_m} \right]_f (\vec{v}_{qp})_f \cdot \vec{S}_f$$

In addition, the relationship given by Eqn. (47) allows to solve the phase fraction transport equation, the third equation in Eqn. (18), using a conservative flux for $\vec{u}$ assembled from the flux of $\vec{v}_m$ given by the last PISO loop.

Given the formulation of the coupled model and the auxiliary equations needed for the pressure-velocity coupling is now possible to describe the solver algorithm for the extended model, which is as follows:

1. Solve the mass conservation equation for the primary phase for α_q^{n+1}, assemble the mass face flux $F_{\rho m}^{n+1}$ and get the new mixture density ρ_m^{n+1} by a loop of `nAlphaSubCycles` cycles where:

   a) The relative velocity at faces is calculated as a flux using Eqn. (38). The calculation of this flux requires to precompute the indicator function θ_f at faces

$$F^{NL,n} = \left[(1 - \theta_f) \, \vec{v}_{rc} \, (\alpha_q^n)^a \right]_f \cdot \vec{S}_f +$$

$$\theta_f \, n_f \min \left[C_\alpha \frac{|\Phi^L|}{|\vec{S}_f|}, \max \left(\frac{|\Phi^L|}{|\vec{S}_f|} \right) \right]$$

   b) The α_q equation [Eqn. (37)] is solved $0 < \nu < $ `nAlphaCorrectors` times by the MULES integrator which also returns the limited flux F_{α_q}. This flux is computed using TVD reconstruction and the *interfaceCompression* scheme for the compressive term.

$$\frac{\alpha_q^{n,\nu+1} - \alpha_q^n}{\Delta t} V + \sum_f F_{\alpha_q} =$$

$$\frac{\alpha_q^{n,\nu+1} - \alpha_q^n}{\Delta t} V + \sum_f \left\{ (\alpha_q^{n,\nu})_f \, F^n + \right.$$

$$\left. [\alpha_q^{n,\nu} \, (1 - \alpha_q^{n,\nu})]_f \, F^{NL,n,\nu} \right\} = 0$$

35

c) The new mass face flux for the present sub-cycle is calculated by Eqn. (44). At the end of the loop the final mass face flux is calculated by Eqn. (45) and the density is updated

$$F_{\rho m, sc, i} = \mathrm{F}_{\alpha_q} \ (\rho_q - \rho_p) + F \, \rho_p \qquad F_{\rho m} = \sum_{i=1}^{n_{sc}} \frac{\Delta t_{sc}}{\Delta t} F_{\rho m, sc, i}$$

$$\rho_m{}^{n+1} = \alpha_q \, \rho_q + (1 - \alpha_q) \, \rho_p$$

2. Solve the momentum predictor [discretized version of the second equation in Eqn. (18)] for $\tilde{\vec{v}}_m$ if the `momentumPredictor` flag is set to `yes`

$$\frac{\rho_m{}^{n+1}\tilde{\vec{v}}_m - \rho_m{}^n \vec{v}_m{}^n}{\Delta t} V + \sum_f F_{\rho m}{}^{n+1} \, \tilde{\vec{v}}_m \cdot \vec{S}_f =$$

$$\sum_f \left(\mu_m{}^{n+1}\right)_f \left(\vec{\nabla}\tilde{\vec{v}}_m\right)_f \cdot \vec{S}_f + \left(\vec{\nabla}\vec{v}_m{}^n \cdot \vec{\nabla}\mu_m{}^{n+1}\right) V$$

$$- \sum_f \left(1 - \theta_f\right) \left[\alpha_q{}^{n+1} \left(1 - \alpha_q{}^{n+1}\right) \frac{\rho_q \, \rho_p}{\rho_m{}^{n+1}} \vec{v}_{qp}{}^n \otimes \vec{v}_{qp}{}^n\right]_f \cdot \vec{S}_f$$

$$+\mathcal{R}\left\{\theta_f \, (\sigma\kappa)_f \left(\vec{\nabla}\alpha_q{}^{n+1}\right)_f - \left[(\vec{g}\cdot\vec{x})_f \left(\vec{\nabla}\rho_m{}^{n+1}\right)_f\right.\right.$$

$$\left.\left. - \left(\vec{\nabla}p_{rgh}{}^n\right)_f\right] |\vec{S}_f|\right\}$$

3. Do the PISO loop $0 < \nu < $ `nCorrectors` times, where:

a) A face flux is calculated using the $H(\vec{v}_m)$ operator with $\tilde{\vec{v}}_m$ obtained in the momentum predictor. This face flux doesn't take into account the effects of the gravity

$$F_{mu}{}^{\nu+1}{}_f = \left(\frac{H\left(\tilde{u}^\nu\right)}{a_P}\right)_f \cdot \vec{S}_f + \mathrm{ddtPhiCorr}(1/a_P, \rho_m, \vec{v}_m{}^\nu, F_m{}^\nu)$$

The flux is then adjusted to obey continuity, via adjustPhi($F_{mu}{}^{\nu+1}, H(\vec{v}_m{}^\nu)/a_P, p_{rgh}{}^\nu$) method

b) The final proposed flux is found adding the effects of of the gravity and the surface tension

$$F_m{}^{\nu+1}{}_f = F_{mu}{}^{\nu+1} + \theta_f \, (\sigma\kappa)_f \left(\vec{\nabla}\alpha_q{}^{n+1}\right)_f$$

$$- (\vec{g}\cdot\vec{x})_f \left(\vec{\nabla}\rho_m{}^{n+1}\right)_f \frac{|\vec{S}_f|}{(a_P)_f}$$

c) The pressure equation is assembled and solved `nNonOrthogonalCorrectors` times for $p_{rgh}{}^{\nu+1}$ in order to circumvent the problem of the gradient calculation in non-orthogonal meshes

$$\sum_f \left[\left(\frac{1}{a_P}\right)_f \left(\vec{\nabla}p_{rgh}{}^{\nu+1}\right)_f\right] \cdot \vec{S}_f = \sum_f F_m{}^{\nu+1}{}_f$$

$$- \sum_f \left[\alpha_q \, (1 - \alpha_q) \frac{\rho_q - \rho_p}{\rho_m}\right]_f (\vec{v}_{qp})_f \cdot \vec{S}_f$$

d) The proposed flux is adjusted by the effect of the pressure and the center-of-volume velocity at the cell centers is adjusted as well

$$F_m{}^{\nu+1}{}_f = F_m{}^{\nu+1}{}_f - \left[\left(\frac{1}{a_P} \right)_f \left(\vec{\nabla} p_{rgh} \right)_f \right] \cdot \vec{S}_f$$

$$\vec{v}_m{}^{\nu+1} = \vec{v}_m{}^{\nu+1} + \frac{1}{a_P} \mathcal{R} \left[\left(F_m{}^{\nu+1}{}_f - F_{mu}{}^{\nu+1}{}_f \right) (a_P)_f \right]$$

e) Finally, the static pressure is reconstructed p from the modified p_{rgh} as $p = p_{rgh} + \rho_m \, \vec{g} \cdot \vec{x}$

4. The face flux for the velocity of center-of-volume is recovered from the flux using Eqn. (47)

$$F^{n+1} = F_m{}^{n+1}{}_f - \left[\alpha_q \, (1 - \alpha_q) \, \frac{\rho_q - \rho_p}{\rho_m} \right]_f (\vec{v}_{qp})_f \cdot \vec{S}_f$$

5. Return to step 1 until finish.

In the first step the α_q is solved. In this stage the MULES integrator is used in order to guarantee the boundedness of α_q and returns the limited value of F_{alpha_q} needed to assemble the mass face flux F_{ρ_m} used in the momentum equation. Next, the momentum predictor is solved in step 2 and the PISO loop is performed in step 3. Each iteration of the PISO loop includes certain number of non-orthogonal corrections to circumvent the issue of implicit gradient calculation in non-orthogonal meshes (Jasak, 1996; Versteeg and Malalasekera, 2007). Finally, in step 4, the flux for the velocity of center-of-volume is recovered in order to be used for the integration of α_q in the next time-step. Thus, the relationship between the velocity of center-of-mass, $\vec{v}_m$, and the velocity of center-of-volume, $\vec{u}$, needed in the system given in Eqn. (18) is expressed in terms of *face fluxes*. From these steps, it is clear that the correct calculation of the flux and its treatment along the solving algorithm plays a central role in the successful implementation of the solver.

The algorithm also includes two methods in the PISO loop: ddtPhiCorr $(1/a_P, \rho_m, \vec{u^\nu}, F^\nu)$ is a flux adjustment due to the time-step needed by the Rhie-Chow interpolation (Choi, 1999), meanwhile adjustPhi$(F_u^{\nu+1}, H(\vec{u}^\nu)/a_P, p_{rgh}^\nu)$

adjusts the flux in free boundaries to obey the continuity equation for $\vec{u}$. Since the presented algorithm is not available in the OpenFOAM® suite it was programmed starting from VOF solver and using the gdbOF debugging tools (Márquez Damián et al., 2012).

5. Examples

In order to validate the proposed method, a series of examples will be solved with both the VOF and the extended methods. The first example corresponds to a bubble plume in laboratory conditions and the objective is to correctly predict the deformation of the free-surface due to the plume and the dynamics of the dispersed phase. This kind of problems is often solved using the Mixture Model; however, the prediction of the free-surface dynamics is not possible since it would be completely smeared. The shape of the free-surface is compared to laboratory experiments and the dynamics of the dispersed phase is qualitatively analyzed. The last two examples have already been presented in the literature, nevertheless, a new insight is given proposing new ways to evaluate the convergence to the DNS solution. So that, the Dam Break problem is revisited comparing the overall behavior of the solutions for both VOF and extended methods. In addition, a measure of the correct dynamics of the dispersed phase is given, allowing the estimation of an improvement factor of the extended model with respect to the VOF model. Finally, the Rayleigh-Taylor instability is calculated using the extended model and the results are compared to VOF solutions. A qualitative comparison of the solutions is made and the dynamics of the dispersed phase in each case is compared using an integrated measure.

5.1. Interaction of a bubble plume with the water surface

The first example gives a semi-quantitative validation from the phenomenon of interaction of a bubble plume and the water surface. This phenomenon appears in blowouts in offshore drilling, broken gas pipelines and natural undersea gas releases forming big bubble plumes. In addition, bubble plumes of small extension are used for mixing process in reservoirs or waste water treatment, chemical reactors and metallurgical processes (Friedl and Fanneløp, 2000; Zanotti, 2007).

The example is taken from the work of Friedl and Fanneløp (Friedl and Fanneløp, 2000) and consists of the generation of a bubble plume in laboratory conditions released from the bottom of a water pool, as is shown in Figure 5. The pool has a square cross-section of 1^1 of side and 0.95 in height. The free surface is set at $H_v = 0.66$. The air is released from the bottom of the tank through a square duct of area $A_i = 0.0005067$ and lenght of $h_i = 0.04502$ with a release velocity of $v_i = 2.6$ which corresponds to the case a4 of the reference. The physical properties of the fluids are as follows: the density of the water, $\rho_q = 1000$, the kinematic viscosity of the water $\nu_q = 1 \times 10^{-6}$, the density of the air $\rho_p = 1$, the kinematic viscosity of the air $\nu_q = 1.48 \times 10^{-5}$ and the surface tension $\sigma = 0.07$. The gravitational acceleration is $\vec{g} = (0, 0, -9.81)$.

As is expected, when the bubble plume reaches the free surface it is disturbed forming a fountain with different shapes but having in common

---

[1]All the magnitudes are expressed in the International System of Units
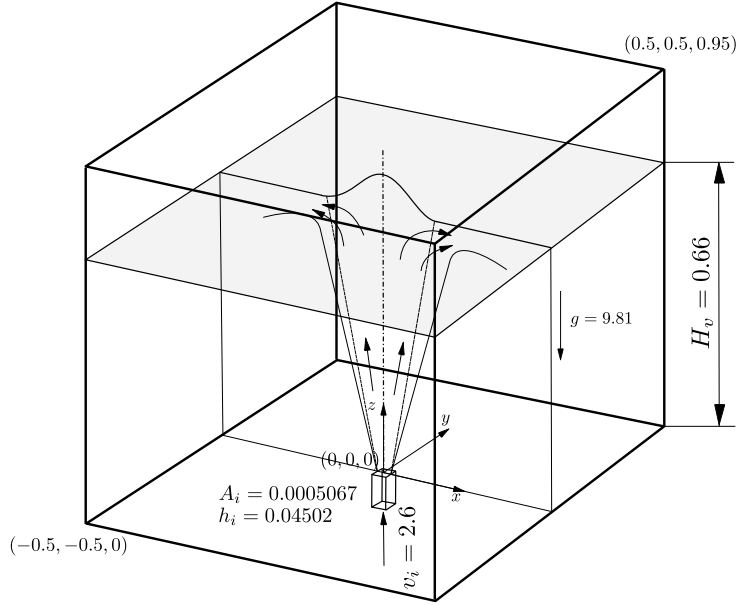
Figure 5: Geometry for the a4 case of bubble plume in (Friedl and Fanneløp, 2000). A_i and h_i are the cross section and height of the inlet duct. The shaded zone indicates the original free surface position and the bell-shaped curve of the mean free surface for the $x - z$ plane
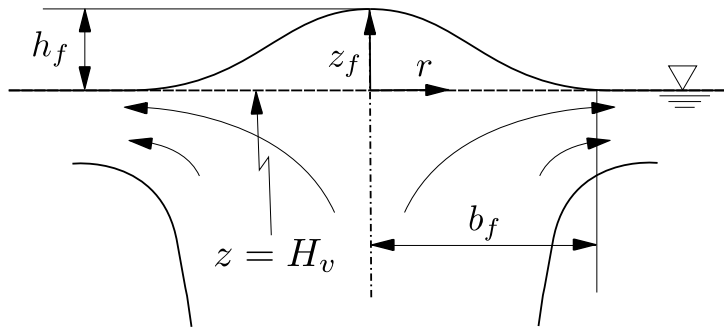
Figure 6: Mean shape of the fountain presented in Figure 5 (adapted from (Friedl and Fanneløp, 2000))

a greater disturbance near the center of the fountain, and then decaying to the sides of the pool, as is shown in Figure 5. The results reported in the reference are an average of the experimental results which can be fitted by a bell-shaped function as in Figure 6. The expression of the mean free surface shape on a given vertical plane ($x - z$ in the figure) is presented in Eqn. (52)

$$h(r) = h_f \, e^{-r^2/b_f^2} \tag{52}$$

where h is the height of the mean free surface for a given radius r (the fountain is considered to be circular), h_f is the maximum height of the fountain and b_f is the semi-diameter of the fountain.

So that, two series of simulations were performed, the first one with the standard VOF solver (`interFoam`[2]) and the second one with the extended model. Each series had three cases with similar settings but with different size hexahedral meshes: a) meshed with `blockMesh` with 364,000 elements; b) meshed in Gambit® with 574,975 elements, with local mesh refinement for a better capturing of the plume and the free surface; c) a mesh resulting of the subdivision by two in the three directions of the previous mesh using the tool `refineMesh`, giving a mesh with 4,599,800 elements and the same refinement properties of the original mesh.

With respect to the boundary conditions for α_q, a zero gradient (`zeroGradient`) was set at all walls except for the top and the inlet. On the top, a mixed boundary condition (`inletOutlet`) was set using a fixed value of zero if the flux is ingoing, and zero gradient for α_q if the flux is outgoing. At the inlet, the

---

[2]The words in courier font corresponds to OpenFOAM®'s utilities or commands

value of α_q was fixed as $\alpha_q = 0$ (`fixedValue`) to ensure a pure air inlet. The boundary conditions for the modified pressure they were set as $\vec{\nabla} p_{rgh} \cdot \vec{S}_f = -\vec{\nabla} \rho \, |\vec{g}| \cdot \vec{S}_f$ (`buoyantPressure`) for all the walls and the inlet. At the top the boundary condition was set with a total pressure (`totalPressure`) of zero. Finally, for the center-of-volume velocity the non-slip boundary condition was set for all walls except for the top and the inlet. At the top the velocity gradient was set as zero for outgoing flows and the value of the velocity as zero for ingoing flows (`pressureInletOutletVelocity`). The inlet was set with a fixed velocity $\vec{u} = (0, 0, 2.6)$ (`fixedValue`). The relative velocity law needed by the zones solved with ASMM in the coupled model was set with $a = 0$, see Eqn. (2), giving a constant velocity. The value for this constant velocity was reported in the reference as $v_{qp} = 0.35$. The parameters for model coupling were set as $\gamma_0 = 0.025$ and $\epsilon = 5 \times 10^{-3}$ after a brief optimization of the results.

The solver was set with the following parameters: `momentumPredictor=no`, `nCorrectors=3`, `nNonOrthogonalCorrectors=0`, `nAlphaCorr=1`, `nAlphaSub Cycles=2`, `cAlpha=1`. The maximum Courant number for this running was set as 0.5, which was larger than the recommended (0.2); in spite of that, it was stable. The first case (VOF with coarse mesh) was run until $t = 10$ in order to reach the full development of the bubble plume; then, it was run to $t = 20$. The left runnings were done mapping the coarse mesh solution for $t = 10$ into the finer meshes and then running until $t = 20$. For all the calculation of the mean values reported for the experiments the interval $t = 10 - 20$ was used.

The general results are reported in Figure 7 for VOF, and in Figure 8 for

the extended model. From the first figure, it is clear that the coarse mesh captures few details of the surface mesh; in addition, the pool has non-physical chunks spread at the sides of the plume (the grayscale has been saturated to white at $\alpha_q = 0.8$ in order to easily see the gas zones). The refinement of the mesh in b) and c) improves the surface capturing but at the same time the VOF method increases its ability to capture the break-up of the big bubbles. The break-up gives small chunks and bubbles which are not correctly removed by buoyancy and then stay in the pool advected by the lateral flow from the plume to the sides. It is expected that successive mesh refinements allow capturing the fine bubbles dynamics, as will be presented for the Dam Break case. The observation of the pictures from the experimental work confirms that the bubbles concentrate around the plume and there is no recirculation (see Figure 3.3 in (Friedl, 1998)). On the other hand, Figure 8 represents the solution for the three meshes with the extended model, where the effect of the mesh refinement is clear again. At the same time, the fragmented chunks are properly removed by the activation of the ASMM giving a clear plume and keeping the pool free of zones without physical meaning.

In addition to this qualitative analysis the shape of the free surface can be compared with the expression given in Eqn. (52). To do so, the void fraction α_q is sampled in 200 points in the interval $0.6 \leqslant z \leqslant 0.8$ on 99 equi-spaced vertical lines in the interval $-0.49 \leqslant x \leqslant 0.49$ on the $x - z$ plane. Then, the transition from zero to one (gas to liquid) is detected giving the position of the free surface (strictly speaking it could capture some droplets from wave splashing, this effect is supposed to be non-determinant). This sampling is
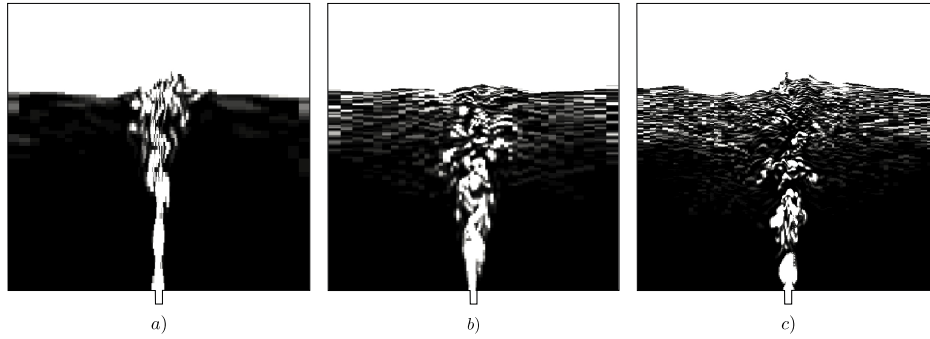
Figure 7: Solution for the bubble plume with VOF for three different meshes, a) coarse, b) fine, c) finest. The grayscale is saturated to white at $\alpha_q = 0.8$
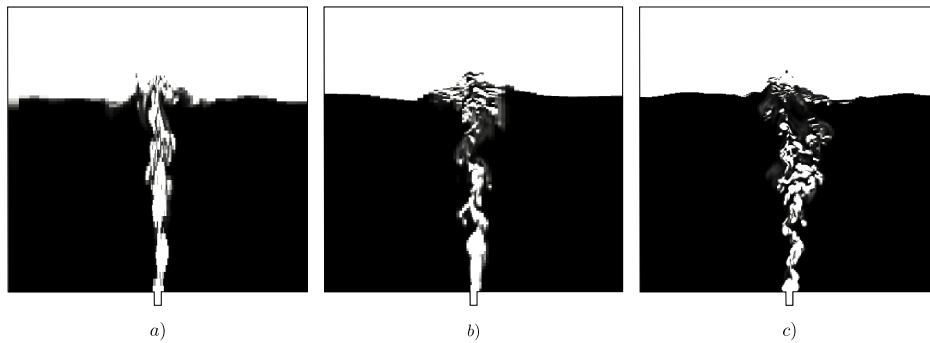

Figure 8: Solution for the bubble plume with the extended model for three different meshes, a) coarse, b) fine, c) finest. The grayscale is saturated to white at $\alpha_q = 0.8$

made with $\Delta t = 0.05$ and then the mean for z values is obtained for each point in x. Finally, the values are referred to the experiments as $\tilde{r} = x_f/b_f$ and $\tilde{z}_f = (z_f - h_{\text{offset}})/h_f$, where h_{offset} allows the adjustment of the offset of profiles respect to the quiescent water level (see Figure 6). The same is made for the bell-shaped function as $\tilde{r} = r/b_f$ and $\tilde{z}_f = h(r)/h_f$, with h_f and b_f are, $h_f = 0.038$ and $b_f = 0.101$. The results are presented in Figure 9, where it is possible to appreciate the effect of the refinement. The reconstruction of the free surface is similar in both of the models showing that the extended method retains the surface capturing capabilities of the VOF model. In addition, comparing the numerical solutions to the experimental fitted curve it is clear that the fountain width is underestimated in both of the models. This effect is attributable to the lack of turbulent dispersion modeling. Here is important to note that the VOF model includes the effects of the turbulence only in the momentum equation in order to model the non-resolved scales of eddies. The scales of the interface are supposed to be captured by the mesh, so no diffusion term is added in the conservation equation of the void fraction.

5.2. Dam Break with degassing

The second example is the Dam Break problem, which is widely used as test problem for multi-phase solvers (Martin and Moyce, 1952; Cruchaga et al., 2007). In this case, a cavity is filled by the less dense fluid and a column of the more dense fluid is formed in a corner. This column suddenly collapses evolving within the cavity with waves and splashing which causes mixing between the fluids. In this case an obstacle has been added in order to
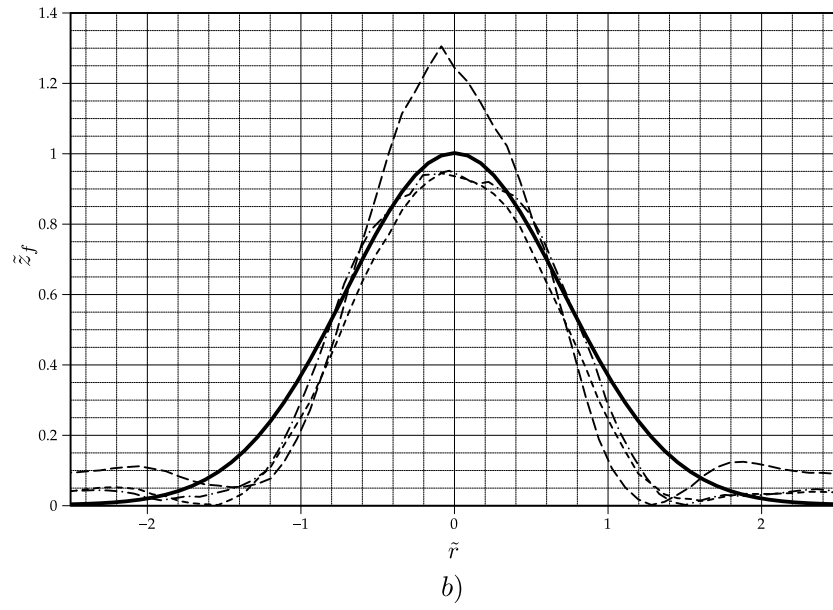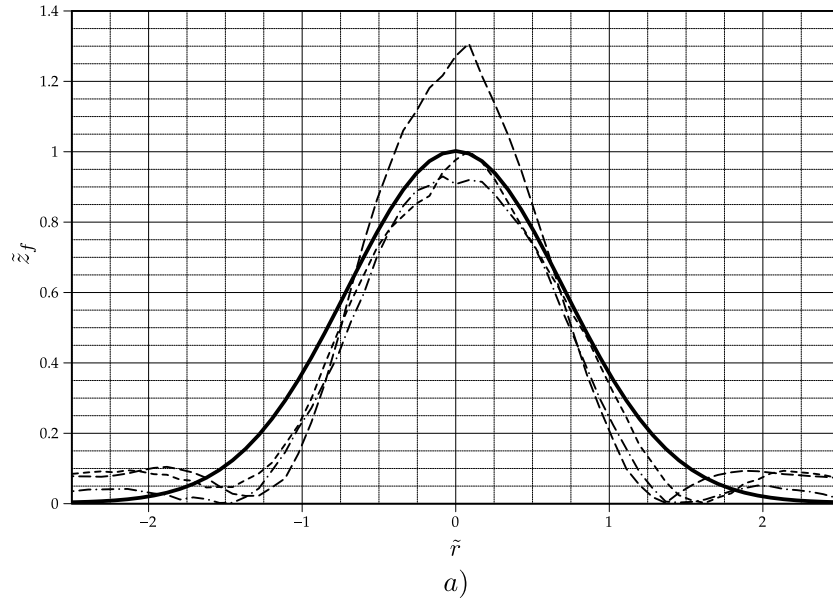
45

Figure 9: Mean surfaces for the bubble plume with a) VOF, b) Extended Model. ▬▬▬ free surface theoretical model; ━ ━ ━ coarse mesh; ▬▬▬▬▬ fine mesh; ━·━·━ finest mesh

assure stronger agitation and mixing. The final state is logically a quiescent pool with the more dense fluid at the bottom and the less dense fluid at the top.

The Dam Break is solved first by the VOF method in the domain $[0,0] \times [0.584, 0.584]$ with an hexahedral mesh of approximately 720×688 (495360) elements, meshed with `blockMesh`, see Figure 10). The physical parameters for the fluids are $\rho_q = 1000$, $\nu_q = 1 \times 10^{-6}$ and $\rho_p = 1$, $\nu_p = 1.48 \times 10^{-5}$ with a surface tension $\sigma = 0.07$. The gravity is set as $\vec{g} = (0, -9.81, 0)$. The solution domain is filled with the less dense fluid except for the area given by $[0,0] \times [0.1461, 0.438]$ where the more dense fluid is located. This rectangle gives the initial condition of the water column that collapses at the beginning of the simulation.

With respect to the boundary conditions for α_q, a zero flux was set in all the walls except for the top where the `inletOutlet` boundary condition was used. In the case of the boundary conditions for the modified pressure, these were set as `buoyantPressure` for all the walls except for the top, where the total pressure boundary condition was set. Finally, for the center-of-volume velocity, the non-slip boundary condition was set for all walls except for the top wall where the `pressureInletOutletVelocity` was used. As the mesh has a dummy third dimension, z, front and back boundaries were set as `empty`, which implies to set as null all the corresponding terms and the derivatives.

The solver was set with the following parameters: `momentumPredictor=no`, `nCorrectors=3`, `nNonOrthogonalCorrectors=0`, `nAlphaCorr=1`, `nAlphaSub Cycles=2`, `cAlpha=1`. The maximum Courant number for this running was

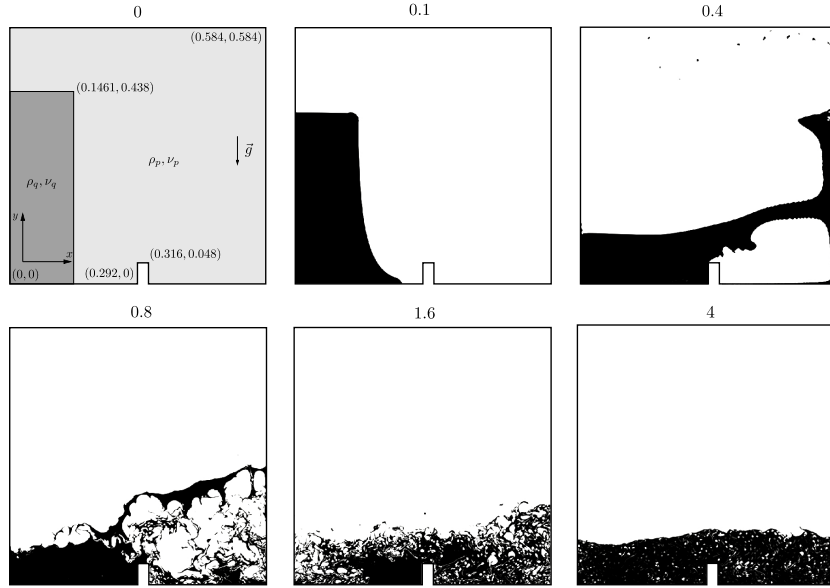set as 0.5, which is greater that the recommended but resulted to be stable.

Figure 10: Evolution of the Dam Break problem

The numerical solution for the Dam Break problem is shown in Figure 10. At the beginning, the more dense fluid column collapses and pass over the obstacle until reach the right wall in a very ordered flow (up to $t = 0.7$, approximately). Once the more dense fluid reaches the right wall, it splashes forming chunks and droplets. The flow oscillates and the interface breaks in several other small interfaces trapping the less dense fluid ($t = 1.6$). The oscillation continues as a liquid pendulum which is damped by the wall and internal friction due to the viscosity ($t \geqslant 3.4$). Finally, the system starts a quiescent stage forming a pool with the more dense fluid at the bottom layer and the less dense fluid trapped in bubbles, which are removed by buoyancy reaching a complete segregated and hydrostatic state (not shown).

It is clear that, after a first stage of mixing, the more dense fluid traps bubbles of the less dense fluid, which are lately removed by buoyancy. At the same time, droplets are formed from the splashing of the waves which fall by the gravity effects. The capacity of the VOF model to capture the physics of these particulated phases is directly related with the mesh refinement, as is shown in Figure 11. In this figure, the solution for the Dam Break problem at $t = 4$ is shown for six different meshes. The first picture ($1\times$) shows the coarsest mesh and then it is successively refined dividing the mesh step by two in both dimensions. The expected effect is observed, as the mesh is refined the reconstruction of the trapped bubbles is improved and the buoyancy is consequently better modeled, so that, the final state as a clean pool is reached more quickly. The improvement in the surface capturing accuracy is also represented. The idea behind the mesh refinement is also to obtain a reference mesh (whenever is possible) which could be considered as a DNS solution of the problem. Since the characteristic size of the bubble population is related to the surface tension this allows to estimate a mean bubble size in order to give a relative velocity law to the ASMM. In addition this size allows to determine from which mesh size is possible to capture the bubbles individually. If the diameter of the bubbles for the Dam Break problem is estimated in 1×10^{-3} the first mesh to start capturing them would be between the $1/32\times$ and $1/64\times$ meshes.

The same analysis can be made for the extended model. It requires the selection of a relative velocity law for the particulated phase. As was stated, the Dam Break problem presents two particulated phases, droplets of the more dense phase and bubbles of the less dense phase. The selection of the

dispersed phase model depends on the detection of which phase is continuous and which phase is dispersed. This is not a trivial problem and is not treated in the available methods. The dispersed phase model is then selected based on a prescribed behavior either as bubbles or droplets. Another option is to use a symmetric law for the dispersed phase model (Černe et al., 2001; Štrubelj and Tiselj, 2011), this approach has validity for $\alpha_q \sim 0.5$ since the drag laws have similar values, but is not completely correct reaching pure phases. From the figures, it is clear that is particularly necessary to give the proper physics to the trapped phase, so that, a bubble model is selected for the relative velocity law with $a = 1$ and $\vec{v}_{rc} = (0, 0.4422, 0)$. Then, the extended model is run with $\gamma_0 = 0.1$ and $\epsilon = 5 \times 10^{-3}$ as the parameters for model coupling. The results are shown in Figure 12 where the effect of the ASMM applied to the dispersed phase is clear, the bubbles are removed giving a clear pool. The mesh refinement effect is also noted in the improvement of the free surface capturing.

The solution for the Dam Break problem is also presented as a validation for the coupled model of Masuda and Nagaoka (Masuda and Nagaoka, 2006) (classic Dam Break, without obstacle). The authors also note the lack of capacity of VOF model to capture the bubbles and droplets and use the Two-Fluid method to give the dynamics for the particulated phase, but no quantitative validation is given with respect to this effect. A possible measure of the bubble removal is to track the inventory of the trapped phase along the time. To this end the solution for each time-step is filtered by p_{rgh} selecting only the cells with $p_{rgh} \geqslant 500$. This threshold was selected in order
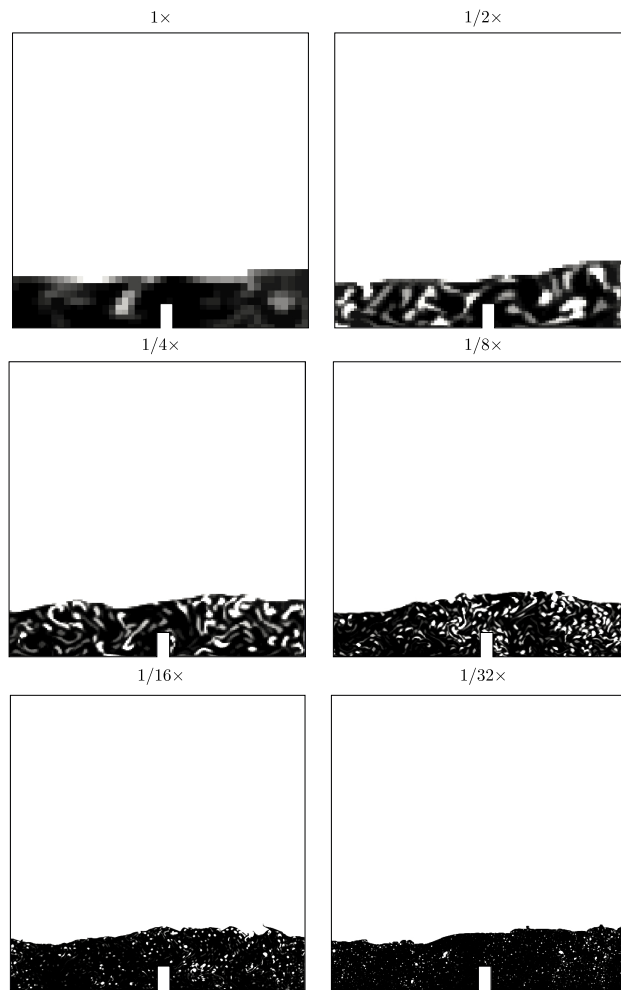
Figure 11: VOF solution for the Dam Break problem at $t = 4$ for different meshes. The grayscale is saturated to white at $\alpha_q = 0.8$
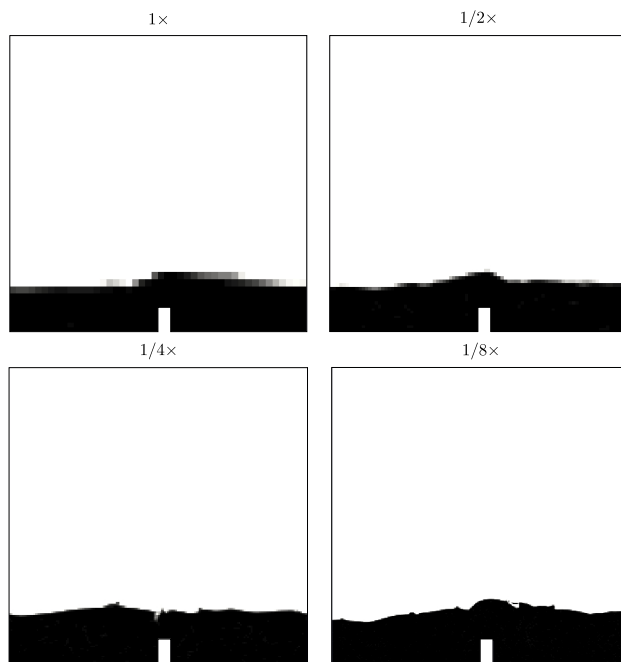
Figure 12: Extended model solution for the Dam Break problem at $t = 4$ for different meshes. The grayscale is saturated to white at $\alpha_q = 0.8$

to capture big extensions of the more dense fluid containing either captured or non captured short scale interfaces with the less dense fluid. This subset of the whole domain is denoted $\mathcal{C}$. So that, the inventory of the less dense fluid is given by $V_p = \sum_{\mathcal{C}} (1 - \alpha_1)$. The results are shown in Figure 13 in linear and semi-logarithmic scale. The semi logarithmic scale in sub-figure b) is given in order to have a better insight of the degassing period from $t \sim 1$.

From the figure is possible to assure that the extended model has better convergence than VOF model, reaching a better degassing without increasing the refinement. It becomes clear comparing the $1/4\times$ solution for the extended model against the $1/32\times$ solution for VOF model. They show similar evolution and close level of degassing at the end of the run, giving an improvement factor of 8. Here it is important to note that the VOF mesh is 64 times larger. Following the argue the $1/8\times$ solution presented for the extended model could only be compared with a $1/256\times$ VOF solution. It implies to go from a problem of 2,008,352 cells ($1/32\times$ case) to another one with 128,534,528 cells, which is only affordable today by large HPC facilities.

5.3. Rayleigh-Taylor instability

The final example corresponds to the Rayleigh-Taylor instability (Štrubelj and Tiselj, 2011), which consists of the evolution of two layers of fluids (see Figure 14). The top layer is more dense than the one placed at the bottom. Due to a little disturbance in the contact surface the more dense fluid goes down and the less dense fluid does the opposite. In the intermediate state, a mixture is created, which is lately segregated. The final state reaches a stable equilibrium with the more dense fluid at the bottom layer and the less
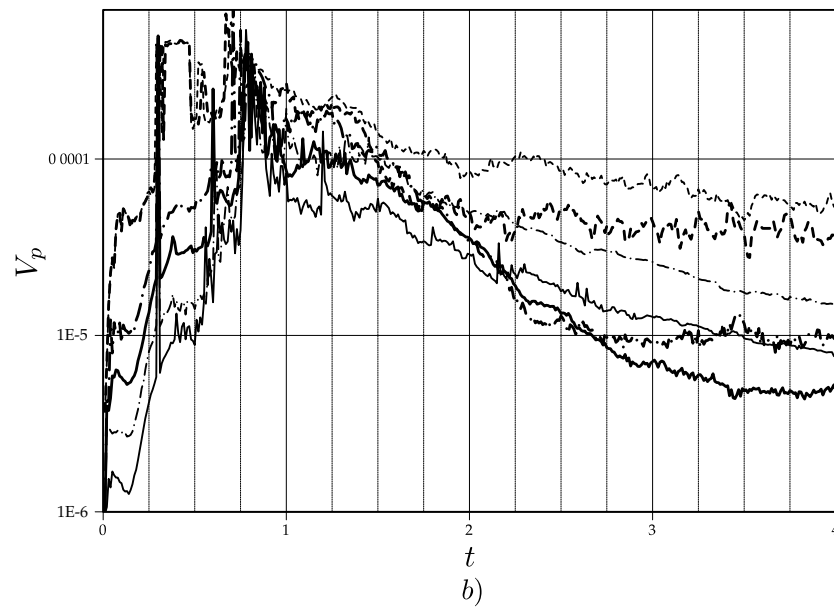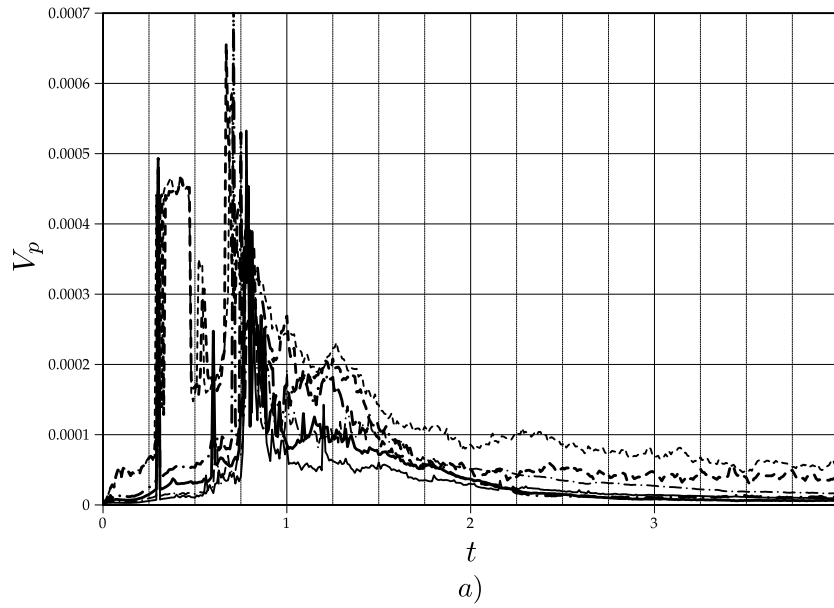
Figure 13: Evolution of the trapped phase volume, V_p, along the time for different meshes and models. a) linear scale, b) semi logarithmic scale. $----$ 1× VOF; $-\cdot-\cdot-$ 1/16× VOF; ——— 1/32× VOF; $-\,-\,-$ 1× extended; $-\cdot-$ 1/4× extended; ——— 1/8× extended

54

dense fluid on the top. The problem is solved in the domain $[0, 0] \times [1, 5]$ with an hexahedral mesh of 128×640 (81920) elements (see Figure 14), which is created using the `blockMesh` utility. The physical parameters for the fluids are $\rho_q = 3$, $\nu_q = 0.01$ and $\rho_p = 1$, $\nu_p = 0.01$, without surface tension. The gravity is set as $\vec{g} = (0, -10, 0)$ and the expression for initial disturbance in the free surface is given by the expression in Eqn. (53), with $\delta_0 = 0.001$

$$\delta = -\delta_0 \left[\cos \left(\frac{2\pi x}{L} - \pi \right) + 1 \right] + 4.5 \tag{53}$$

The shape of the initial disturbance is followed by the mesh on the interface zone since the size of the deformation is smaller than the mesh step. This small size impedes to set the initial disturbance only by cell initialization. With respect to the boundary conditions for α_q, `zeroGradient` was set at the top and bottom boundaries of the domain and symmetry conditions at both sides. The same boundary conditions were set for the modified pressure and a pressure reference point was set at $(0.4999, 0.00078125, 0)$ with $p = 0$. Finally, the boundary conditions for the velocity were set as non-slip for top and bottom boundaries and symmetry conditions at both sides. As the mesh has a dummy third dimension, z, front and back boundaries were set as `empty`.

The solver was set with the following parameters: `momentumPredictor=yes`, `nCorrectors=3`, `nNonOrthogonalCorrectors=1`, `nAlphaCorr=1`, `nAlphaSub Cycles=2`, `cAlpha=0.25`. The value of `cAlpha` was selected in order not to form spurious ripple in the free surface when the big structures of the flow are being stretched. The time-step was set as $\Delta t = 0.0001$ which assured a Courant number below 0.1 in all the run and was proper for the development

of the mushroom-like structure at the beginning.

The results for the VOF method are presented in Figure 14 for several times. The evolution starts with the development of a mushroom-like structure, until approximately $t = 1.8$. After this time the structure is stretched and filaments start to detach forming isolated chunks (see Figure 14 at $t = 2.7$, $t = 3.6$). The detaching continues keeping only chunks and filaments, some of these chunks are fragmentated in a size not trackable by the VOF method. At the end, a sedimentation process starts where the more dense chunks fall as droplets, and the less dense fluid trapped in the bottom layer escapes by buoyancy as bubbles. The final state (not shown) is clearly a layered solution with the more dense fluid forming the bottom layer. So that, after a first stage when the solution evolves with a mushroom-like structure ($t < 1.8$) the problem turns into the stretching of these structures ($t < 4.5$) and eventually the formation of droplets ($t \cong 1.8$). The dynamics of this particulate phase can be correctly modeled by the VOF method with greater or lesser detail depending on the mesh size. So that, the principal idea behind the use of an extended model is to give the proper physics to the particulate phase in order to have a better prediction, using the same meshes.

In order to evaluate the behavior of the extended model with respect to VOF, the Rayleigh-Taylor problem was run with VOF in a reference mesh of 256×1280 (327,680) elements. This mesh is a refined version of the base mesh presented as the VOF example, dividing each cell by two in both x and y directions. So that, the base is called $1\times$, and the reference is called $1/2\times$. The series is completed with coarser meshes, which are called $2\times$ and $4\times$.
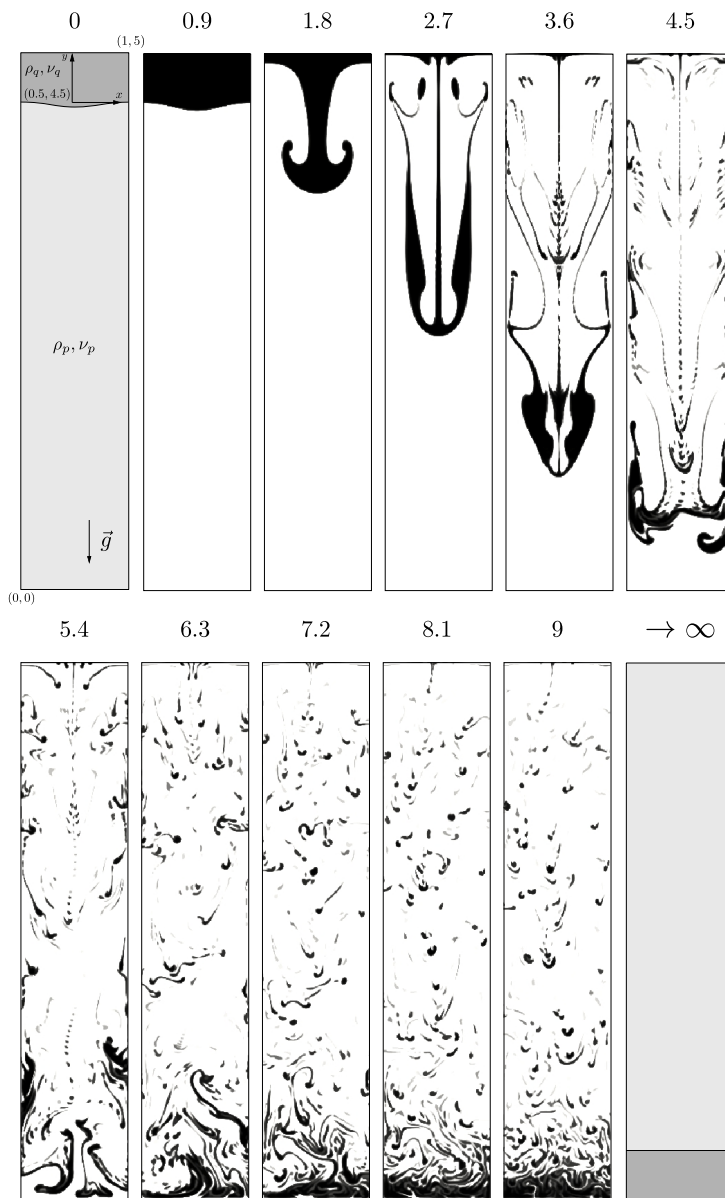
Figure 14: Evolution of the Rayleigh-Taylor instability

The problem is then run for VOF and extended models for all the meshes using the boundary conditions selected for the original VOF example. In the extended model, the parameters for the indicator function are $\gamma_0 = 0.1$ and $\epsilon = 5 \times 10^{-3}$. The relative velocity law needed for the ASMM module in the extended model is adjusted to $\vec{v}_{rc} = (0, -0.1, 0)$ and $a = 1$ from the results in the reference mesh. The results are shown in Figure 15 for three different times $t = 1.8$, $t = 3.6$ and $t = 9$. In each time row the results for all meshes are shown comparing each VOF $(n\times)$ solution with this extended model pair $(n \times e)$. The first row corresponds to the end of the linear period, the second shows the stretching of the original structures and the presence of fluid chunks; finally the third row shows the falling droplets stage and the formation of the bottom pool. From the figure, it is clear that the linear period is well represented by both methods in all of the meshes, since the mushroom-like structure is formed by long-scale interfaces. The stretching of the original structures shows the deficiencies of the coarser meshes where non-physical fluid chunks start to appear. Finally, in the droplets/pool stage it is clear that the VOF method tries to agglomerate the chunks meanwhile the extended model, which is working in ASMM regime, treats the chunks without taking into account the mesh resolution.

In order to compare the solution quantitatively, the quadratic mean error is calculated for the $4\times$, $2\times$ and $1\times$ respect to the $1/2\times$ reference mesh for both methods. In order to do so, all the results are mapped to the coarsest mesh. The error is calculated as is shown in Eqn. (54) (Černe et al., 2001).
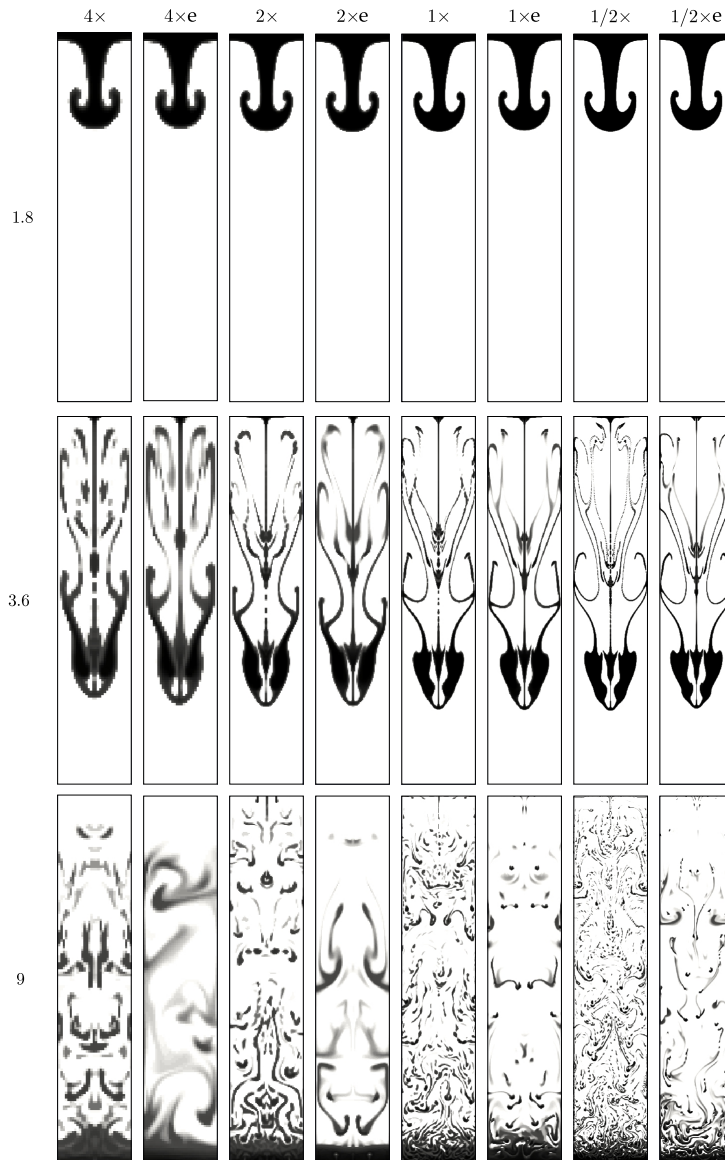
Figure 15: Extended model solution for the Dam Break problem at $t = 4$ for different meshes and methods. The grayscale is saturated to black at $\alpha_q = 0.16$

$$\delta_{\text{cell}}(t) = \frac{1}{V_R} \sum_{i=1}^{n} [\alpha_q(t) - \alpha_{q,REF}(t)]_i^2 \tag{54}$$

where i is the index for the cells, n is the total number of cells in the mesh and $V_R = \sum_{i=1}^{n} \alpha_{q,REF}(t)$. The results are presented in Figure 16 and show that the effects of the mesh refinement are clear until $t \sim 4.5$. In this period, as the meshes are finer the solution is more accurate. This behavior is similar for both VOF and extended models. In addition, each VOF solution is followed by its extended model pair showing the capacity of extended model to capture the long-scale interfaces, while the mesh remains fine with respect to the interface scale. Once the big structures are stretched and the droplets are formed, the convergence in not completely clear.
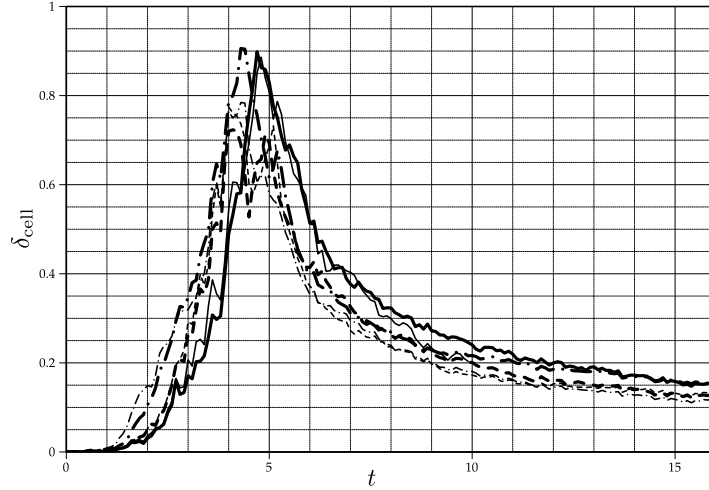

Figure 16: Quadratic mean error for VOF and extended model solutions respect to VOF reference for the Rayleigh-Taylor problem. ▬▬ 1× VOF , ▬ ▬ ▬ 2× VOF, ▬ · ▬ 4× VOF,▬▬ 1× extended ,------· 2× extended, ▬·▬·▬ 4× extended

60

Another quantitative validation is given by the accumulation of the more dense phase in the bottom of the domain. It gives a measure of the correct capturing of the falling droplets physics. So that, the integral of α_q is calculated in a box with its upper boundary located at $y = 0.5$ for all of the times. The results shown in Figure 17 allow to conclude again that the VOF and extended model behave similarly; nevertheless, the extended model seems to converge better in a factor of 2, since the results for $2\times$ in the extended model are comparable to the results for $1\times$ in VOF. The same conclusion is obtained comparing the results in $1\times$ in the extended model and the results for $1/2\times$ in VOF.
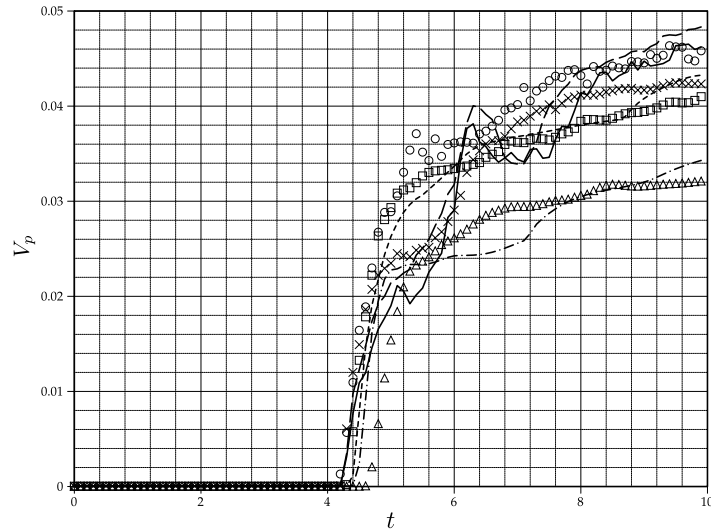

Figure 17: Accumulation of the more dense phase at the bottom of the domain for the Rayleigh-Taylor problem. ○ $1/2\times$ VOF, × $1\times$ VOF, □ $2\times$ VOF, △ $4\times$ VOF, ——— $1/2\times$ extended, — — — $1\times$ extended, ⁃⁃⁃⁃⁃ $2\times$ extended, —·—·— $4\times$ extended

6. Conclusions

In this work, an extended mixture model was presented and a high performance solver was implemented and tested in order to solve problems with different scales in the interface based on the ASMM and VOF models. To derive such model, a discussion was set about the similarities between ASMM and VOF, showing that the later can be completely derived from the first. This characteristic allowed to obtain an unified solving framework with strong coupling between the base methods and to preserve the original characteristics in the treatment of the interfaces. So that, the large scale interfaces continued to be properly captured by means of the VOF method and the short scale interfaces dynamics were treated by the ASMM. The implementation by the FVM required a careful treatment of the face fluxes in order to obtain a conservative method, this topic was explained in the theory fundamentals and was used as a key concept to devise the solver algorithm. In addition, an indicator function was presented to allow the correct coupling of both ASMM and VOF methods with a low demanding technique.

As a part of the discussion, a description of the state of the art was given in order to have a better understanding of the scope and limitations of the known coupled solvers, including the development of new theoretical and experimental solutions which allow the validation of the models.

The model was applied to three examples. The first one was an experimental bubble plume taken from the literature, giving place to a new test case. The solution of this case allowed to have a semi-quantitative validation based on the inspection of the solution and the comparison of the shape of the free-surface. This last comparison was made against fitting curves based

on experimental results. The results allowed to affirm that the coupled model could correctly capture the large scale interfaces given by the pool's water surface and the fountain. The diameter of the fountain was slightly underestimated, which is attributable to the lack of turbulent diffusion in the dispersed phase. Here it is important to note that the coupled model can easily be updated including turbulent diffusion in the secondary phase mass conservation equation, which cannot be made in the VOF method since all interface scales are supposed to be solved. In addition, the trapped bubbles present in the pool, which couldn't be removed by buoyancy forces by the VOF method, were properly removed adding the correct physics by the ASMM. This effect allowed to match the observed experimental results.

The second example relied on the Dam Break problem, it was solved with the extended method and a comparison was done against the VOF model which is the typical method used to solve it. An eight times improvement was found related to mesh requirements based on a novel quantitative comparison based on the mass of the trapped phase. The final example was the Rayleigh-Taylor instability where the extended model was compared to VOF, showing again the capacity of correctly capture the big structures giving the same performance than VOF. In a second stage, where the problem evolves as particulated phases, the extended model gave an improvement factor of two. As a measure of the improvement, the accumulation of the primary phase at the bottom of the domain was tracked. These last two examples have been solved by other authors being a part of the typical test for coupled model. In both cases, the proposed method showed comparable results to other methods and the utilization of improved measures allows to have more

tools to evaluate the convenience of the coupled models.

As is usual, the examination of the benefits and deficiencies of this kind of methods leave some open questions to the community. An open question which deserves much attention and which has not been discussed is related to the interaction of the short scale interfaces (SSI) and the large scale interfaces (LSI). From the given examples, it is clear that the dynamics of the SSI is improved, now is necessary to know how the LSI simulation is improved due to the better calculation of the SSI. This question is not so trivial to answer since requires very accurate validation data either theoretical or experimental.

7. Acknowledgments

References

Babik, F., Gallouët, T., Latché, J., Suard, S., Vola, D.. On two fractional step finite volume and finite element schemes for reactive low mach number

flows. In: The International Symposium on Finite Volumes for Complex Applications IV-Problems and Perspectives-Marrakech (2005). 2005. .

Berberovic, E., Van Hinsberg, N., Jakirlic, S., Roisman, I., Tropea, C.. Drop Impact onto a Liquid Layer of Finite Thickness: Dynamics of the Cavity Evolution. Physical Review E 2009;79.

Bohorquez, P.. Finite volume method for falling liquid films carrying monodisperse spheres in newtonian regime. AIChE Journal 2012;58(8):2601–2616.

Brackbill, J., Kothe, D., Zemach, C.. A continuum method for modeling surface tension. Journal of Computational Physics 1992;100(2):335–354.

Brennen, C.E.. Fundamentals of multiphase flow. Cambridge University Press, 2005.

Carrica, P., Wilson, R., Stern, F.. An unsteady single-phase level set method for viscous free surface flows. International Journal for Numerical Methods in Fluids 2006;53(2):229–256.

Choi, S.. Note on the use of momentum interpolation method for unsteady flows. Numerical Heat Transfer: Part A: Applications 1999;36(5):545–550.

Cloete, S., Olsen, J., Skjetne, P.. CFD modeling of plume and free surface behavior resulting from a sub-sea gas release. Applied Ocean Research 2009;31(3):220–225.

Cruchaga, M., Celentano, D., Tezduyar, T.. Collapse of a Liquid Col-

umn: Numerical Simulation and Experimental Validation. Comput Mech 2007;39:453–476.

Drew, D.. Mathematical Modeling of Two-phase Flow. Annual Review of Fluid Mechanics 1983;15(1):261–291.

Friedl, M.. Bubble plumes and their interactions with the water surface. Ph.D. thesis; Swiss Federal Institute of Technology (ETH), Zürich; 1998.

Friedl, M., Fanneløp, T.. Bubble plumes and their interaction with the water surface. Applied Ocean Research 2000;22(2):119–128.

Gastaldo, L., Herbin, R., Latché, J.. An entropy preserving finite-element/finite-volume pressure correction scheme for the drift-flux model. Arxiv preprint arXiv:08032469 2008;.

Gastaldo, L., Herbin, R., Latché, J.. A discretization of the phase mass balance in fractional step algorithms for the drift-flux model. IMA Journal of Numerical Analysis 2011;31(1):116–146.

Gopala, V., van Wachem, B.. Volume of Fluid Methods for Immiscible-fluid and Free-surface Flows. Chemical Engineering Journal 2008;141(1-3):204–221.

Hirsch, C.. Numerical computation of internal and external flows: fundamentals of computational fluid dynamics. volume 1. Butterworth-Heinemann, 2007.

Hirt, C., Nichols, B.. Volume of Fluid (VOF) Method for the Dynamics of Free Boundaries. Journal of Computational Physics 1981;39:201–225.

66

Ishii, M.. Thermo-Fluid Dynamic Theory of Two-phase Flow. NASA STI/Recon Technical Report A 1975;75.

Ishii, M., Hibiki, T.. Thermo-fluid dynamics of two-phase flow. Springer Verlag, 2010.

Issa, R.. Solution of Implicitly Discretised Fluid Flow Equations by Operator Splitting. Journal of Computational Physics 1986;62:40–65.

Jasak, H.. Error analysis and estimation for the finite volume method with applications to fluid flows. Ph.D. thesis; Department of Mechanical Engineering Imperial College of Science, Technology and Medicine, London, UK; 1996.

Knio, O., Najm, H., Wyckoff, P.. A semi-implicit numerical scheme for reacting flow: II. Stiff, operator-split formulation. Journal of Computational Physics 1999;154(2):428–467.

Kolev, N.. Multiphase Flow Dynamics 4: Nuclear Thermal Hydraulics. Springer-Verlag GmbH, 2010.

Bohorquez R. de M., P.. Study and Numerical Simulation of Sediment Transport in Free-Surface Flow. Ph.D. thesis; Málaga University, Málaga; 2008.

Manninen, M., Taivassalo, V., Kallio, S.. On the mixture model for multiphase flow. Technical Research Centre of Finland, 1996.

Márquez Damián, S.. An extended mixture model for the simultaneous treat-

ment of short and long scale interfaces. Ph.D. thesis; FICH, Universidad Nacional del Litoral, Santa Fe, Argentina; 2013.

Márquez Damián, S., Giménez, J., Nigro, N.. gdbOF: A debugging tool for openFOAM®. Advances in Engineering Software 2012;47(1):17–23.

Martin, J., Moyce, W.. An Experimental Study of the Collapse of Liquid Columns on a Rigid Horizontal Plane. Philos Trans R Soc Lond 1952;244:312–324.

Masuda, R., Nagaoka, M.. A Coupled Interface-capturing and Multi-fluid Model Method for Computing Liquid Jet from Nozzle Flow. In: International Congress on Liquid Atomization and Spray Systems (2006). 2006. .

Najm, H., Wyckoff, P., Knio, O.. A semi-implicit numerical scheme for reacting flow: I. Stiff chemistry. Journal of Computational Physics 1998;143(2):381–402.

OpenCFD, . OpenCFD Technical report no. TR/HGW/02. 2005.

Peng Karrholm, F.. Numerical Modelling of Diesel Spray Injection, Turbulence Interaction and Combustion. Ph.D. thesis; Chalmers University of Technology, Goteborg; 2008.

Prosperetti, A., Tryggvason, G.. Computational methods for multiphase flow. Cambridge University Press, 2007.

Puckett, E., Almgren, A., Bell, J., Marcus, D., Rider, W.. A high-order projection method for tracking fluid interfaces in variable density

incompressible flows. Journal of Computational Physics 1997;130(2):269–282.

Rhie, C.M., Chow, W.L.. Numerical study of the turbulent flow past an airfoil with trailing edge separation. AIAA Journal 1983;21(11):1525–1532.

Rider, W., Kothe, D.. Reconstructing volume tracking. Journal of Computational Physics 1998;141(2):112–152.

Rudman, M.. Volume-tracking Methods for Interfacial Flow Calculations. International Journal for Numerical Methods in Fluids 1997;24(7):671–691.

Rusche, H.. Computational Fluid Dynamics of Dispersed Two-Phase Flows at High Phase Fractions. Ph.D. thesis; Imperial College of Science, Technology and Medicine, London; 2002.

Scardovelli, R., Zaleski, S.. Direct Numerical Simulation of Free-Surface and Interfacial Flow. Annual Review of Fluid Mechanics 1999;31(1):567–603.

Schiller, L., Naumann, Z.. A drag coefficient correlation. Z Ver Deutsch Ing 1935;77:318.

Trontin, P., Vincent, S., Estivalezes, J., Caltagirone, J.. Detailed comparisons of front-capturing methods for turbulent two-phase flow simulations. International Journal for Numerical Methods in Fluids 2008;56(8):1543–1549.

Tryggvason, G., Esmaeeli, A., Lu, J., Biswas, S.. Direct Numerical Simulations of Gas/liquid Multiphase Flows. Fluid Dynamics Research 2006;38(9):660–681.

Černe, G., Petelin, S., Tiselj, I.. Coupling of the Interface Tracking and the Two-fluid Models for the Simulation of Incompressible Two-phase Flow. Journal of Computational Physics 2001;171:776–804.

Versteeg, H., Malalasekera, W.. An introduction to computational fluid dynamics: the finite volume method. Prentice Hall, 2007.

Štrubelj, L., Tiselj, I.. Two-fluid Model with Interface Sharpening. International Journal for Numerical Methods in Engineering 2011;85(5):575–590.

Weller, H.. A new approach to VOF-based interface capturing methods for incompressible and compressible flow. 2008.

Weller, H., Tabor, G., Jasak, H., Fureby, C.. A Tensorial Approach to Computational Continuum Mechanics Using Object-oriented Techniques. Computers in Physics 1998;12:620.

Yan, K., Che, D.. A Coupled Model for Simulation of the Gas-liquid Two-phase Flow with Complex Flow Patterns. International Journal of Multiphase Flow 2010;36(4):333–348.

Zalesak, S.. Fully Multidimensional Flux-Corrected Transport Algorithms for Fluids. Journal of Computational Physics 1979;31:335–362.

Zanotti, A., Mendez, C., Nigro, N., Storti, M.. A Preconditioning Mass Matrix to Avoid the Ill-posed Two-fluid Model. Journal of Applied Mechanics 2007;74:732.

Zanotti, A.L.. Modelado del Flujo Multifase en la Produccion de Acero por

Colada Continua. Ph.D. thesis; Facultad de Ingeniería y Ciencas Hídricas, UNL. Santa Fe, Argentina; 2007.